

Assessment of climate change impacts at the catchment scale with a detailed hydrological model of surface-subsurface interactions and comparison with a land surface model

M. Sulis,¹ C. Paniconi,¹ C. Rivard,² R. Harvey,³ and D. Chaumont⁴

Received 1 February 2010; revised 20 October 2010; accepted 26 October 2010; published 28 January 2011.

[1] A process-based model that incorporates hydrodynamic feedbacks between the land surface, soil, and groundwater zones is used to assess the sensitivity of the hydrological response (river discharge, aquifer recharge, and soil water storage) to future climate conditions. The analysis is based on the Intergovernmental Panel on Climate Change Special Report on Emissions Scenario A2 and the des Anglais catchment in southwestern Quebec (Canada). Application of the coupled hydrological model (CATHY) to the study basin revealed significant spatiotemporal variations in the river discharge response to climate change owing to a different partitioning between the overland runoff and base flow components of the hydrograph, with the latter alleviating the marked decrease in discharge during the summer period. A spatial analysis of recharge patterns shows that the greatest variations are expected to occur, throughout the year, in the southern portion of the catchment, where the elevations are highest. Compared to river discharge and aquifer recharge, the soil water storage volumes are less sensitive to climate changes. From a spatial analysis of soil moisture variations it was possible to observe organizational patterns that follow the topographic and pedologic characteristics of the catchment. In addition to these analyses, we also compare predictions obtained with the land surface scheme (CLASS) that is coupled to the regional climate model (CRCM) to those from the detailed catchment model for past and future climate change projections. An examination of the runoff revealed that CLASS produces higher estimates than CATHY of surface and subsurface runoff throughout the annual cycle for both past and future projections. For soil water storage, the two models are in general agreement in terms of the intra-annual variability of moisture content at shallower soil layers, whereas a larger difference is found for the deepest layer, with CATHY predicting wetter soil conditions over the entire simulation period and moisture fluctuations of much smaller amplitude.

Citation: Sulis, M. C. Paniconi, C. Rivard, R. Harvey, and D. Chaumont (2011), Assessment of climate change impacts at the catchment scale with a detailed hydrological model of surface-subsurface interactions and comparison with a land surface model, *Water Resour. Res.*, 47, W01513, doi:10.1029/2010WR009167.

1. Introduction

[2] The Intergovernmental Panel on Climate Change (IPCC) has found evidence that recent regional climate changes, particularly temperature increases, have already affected many physical and biological systems [IPCC, 2007]. General circulation models (GCMs), aided by appropriate downscaling techniques, have long been used to simulate changes in regional climate systems over wide spatiotemporal scales and to allow information from large-

scale atmospheric simulations to be used in smaller-scale hydrological models [Wilby and Wigley, 1997; Arnell *et al.*, 2003].

[3] Changes in future climate will alter regional hydrological cycles with subsequent impact on the quantity and quality of regional water resources [Gleick, 1989]. While climate change affects surface water directly through changes in long-term climate variables, the impacts on groundwater are more difficult to assess [Jyrkama and Sykes, 2007]. To address this issue a number of studies have been undertaken. Dooge *et al.* [1999] explored the sensitivity of runoff to climate change for three scenarios using a very simple hydrological model. Arora and Boer [2001] studied the impact of future climate change on the hydrology of 23 major river basins using a GCM coupled to a river routing algorithm that included surface and groundwater reservoirs. Caballero *et al.* [2007] investigated the sensitivity during low-flow periods of a regional-scale basin with a hydrometeorological modeling system. York *et al.* [2002] and Scibek and Allen [2006] studied

¹Centre Eau, Terre et Environnement, Institut National de la Recherche Scientifique, Université du Québec, Québec, Canada.

²Geological Survey of Canada, Québec, Canada.

³Climate Research Branch, Environment Canada at Ouranos, Montreal, Canada.

⁴Ouranos Consortium on Regional Climatology and Adaptation to Climate Change, Montreal, Canada.

climate change impacts on groundwater recharge, while *Tague et al.* [2008] highlighted the role of groundwater in maintaining base flow under an altered climate. *Quilbé et al.* [2008] and *van Roosmalen et al.* [2009] examined the combined effects of future climate and land use changes on agricultural watersheds. Despite these studies, very few assessments of climate change impacts on freshwater resources have been conducted using fully coupled numerical models that consider the important hydrodynamic feedbacks between the land surface, soil, and groundwater zones.

[4] Interactions between surface and subsurface water play a critical role in the hydrological cycle [e.g., *Liang et al.*, 2003; *Gulden et al.*, 2007; *Maxwell et al.*, 2007]. Improving the representation of infiltration and soil moisture processes in current land surface models is considered essential for accurate simulation of energy and moisture fluxes. Soil moisture plays a key role in partitioning precipitation into infiltration, surface runoff, and drainage to groundwater, and it also controls the partitioning of energy into sensible and latent heat fluxes at the ground surface, affecting the coupling between the land surface and the atmospheric boundary layer [*Brubaker and Entekhabi*, 1996; *Eltahir*, 1998]. Although land surface models have evolved from simple [*Manabe et al.*, 1965] to more sophisticated parameterizations [*Lee and Abriola*, 1999; *Wang et al.*, 2002; *Pitman*, 2003; *Yeh and Eltahir*, 2005], they are still limited to vertical moisture transport in the soil column and lack an adequate representation of surface and subsurface lateral transport due to topography or moisture gradients. Lateral processes and a better surface–subsurface coupling, commonly considered at small hillslope and catchment scales [*Singh and Woolhiser*, 2002; *Furman*, 2008], can also play an important role at larger regional scales, especially if latent heat flux–soil moisture feedbacks and shallow water table dynamics are embedded in fully integrated hydrometeorological models [*Fan et al.*, 2007; *Kollet and Maxwell*, 2008].

[5] This work presents an assessment of climate change impacts for a medium-sized catchment (690 km²) based on numerical simulations with a coupled physically based model of surface and groundwater flow. A distributed model of this type allows us to investigate in detail the role of feedbacks between near-surface and deeper hydrological processes, the influence of factors such as topography and subsurface heterogeneity in amplifying or attenuating eventual impacts, and the ways in which processes that control the catchment dynamics can be altered in response to climate changes. The study area is the des Anglais river basin located in southwestern Quebec (Canada). The future climate projection (2041–2070) was constructed by applying, to an observed daily data set (1961–1990), a monthly deviation factor extracted from projections generated by the Canadian Regional Climate Model (CRCM) [*Music and Caya*, 2007]. This approach eliminates biases in the climate simulations (differences between observed and simulated climate), especially in precipitation, and it allows incorporation of detailed meteorological information contained in site-specific data [*Rivington et al.*, 2008].

[6] An additional objective of this study was to compare results from the process-based catchment hydrological model with those obtained from the land surface model that

has recently been coupled to the CRCM. Land surface schemes have been extensively evaluated against observed data and through intercomparison studies [e.g., *Bowling et al.*, 2003; *Boone et al.*, 2004]. For the des Anglais study, the surface–subsurface runoff and soil water predictions obtained from the Canadian Land Surface Scheme (CLASS) [*Verseghy*, 1991; *Verseghy et al.*, 1993] are compared to those obtained with the Catchment Hydrology (CATHY) coupled groundwater–surface water model [*Camporese et al.*, 2010]. The size of the study area, relatively large for a detailed surface–subsurface model and comparatively small for a land surface model, is a convenient spatial scale at which to investigate the importance of a three-dimensional representation of a catchment that takes into account a mathematical description of surface and subsurface processes and of factors such as topography and water table dynamics.

2. Study Area

[7] The des Anglais river basin (Figure 1) has a drainage area of 690 km² and an average discharge of 300×10^6 m³ per year at its outlet. It is the largest subcatchment of the transboundary Chateauguay River watershed and has an elevation range from 30 to 400 m. The Chateauguay basin constitutes the northern part of the Adirondack mountain range and initiates the physiographical region of the St. Lawrence Platform. The aquifer system in this region is part of the St. Lawrence Lowlands and consists of Cambrian to Middle Ordovician sedimentary rocks that are slightly deformed and fractured. Unconsolidated sediments of glacial and postglacial origin (Wisconsinan period and Champlain sea event) overlay the bedrock aquifer and are of varying thickness, reaching 40 m in the northernmost portion [*Tremblay*, 2006]. These sediments are, in turn, overlain by Quaternary deposits of silty till, compact and dense at the base and reworked and more permeable above. The soils are characterized as mainly weathered Quaternary sediments [*Lamontagne*, 2005], with the exception of bogs and swamps that overlie Champlain sea sediments in the northeastern part of the catchment. These wetlands correspond to closed depressions with a thick accumulation of organic material.

[8] Water table fluctuations in the des Anglais catchment are mainly driven by springtime snowmelt and by rainfall in the fall. The groundwater recession typically extends from June to the end of the growing season (September–October). Mean annual water table fluctuations are about 2.7 m under unconfined or semiconfined conditions and about 1.6 m under confined conditions [*Côté et al.*, 2006]. The study area belongs to the Great Lakes and St. Lawrence climate region, characterized by a semihumid climate with cold winters and humid summers. The annual mean temperature is 6.3°C, with monthly variations from –10°C in January to 20°C in July (Environment Canada, Canadian daily climate data (CDCD), 2004, <http://climate.weatheroffice.ec.gc.ca>). These temperatures result in frost conditions from mid-November to the end of March. The average annual precipitation is 958 mm, relatively uniformly distributed within the watershed, with snowfall prevalent from December to March when temperatures are below 0°C.

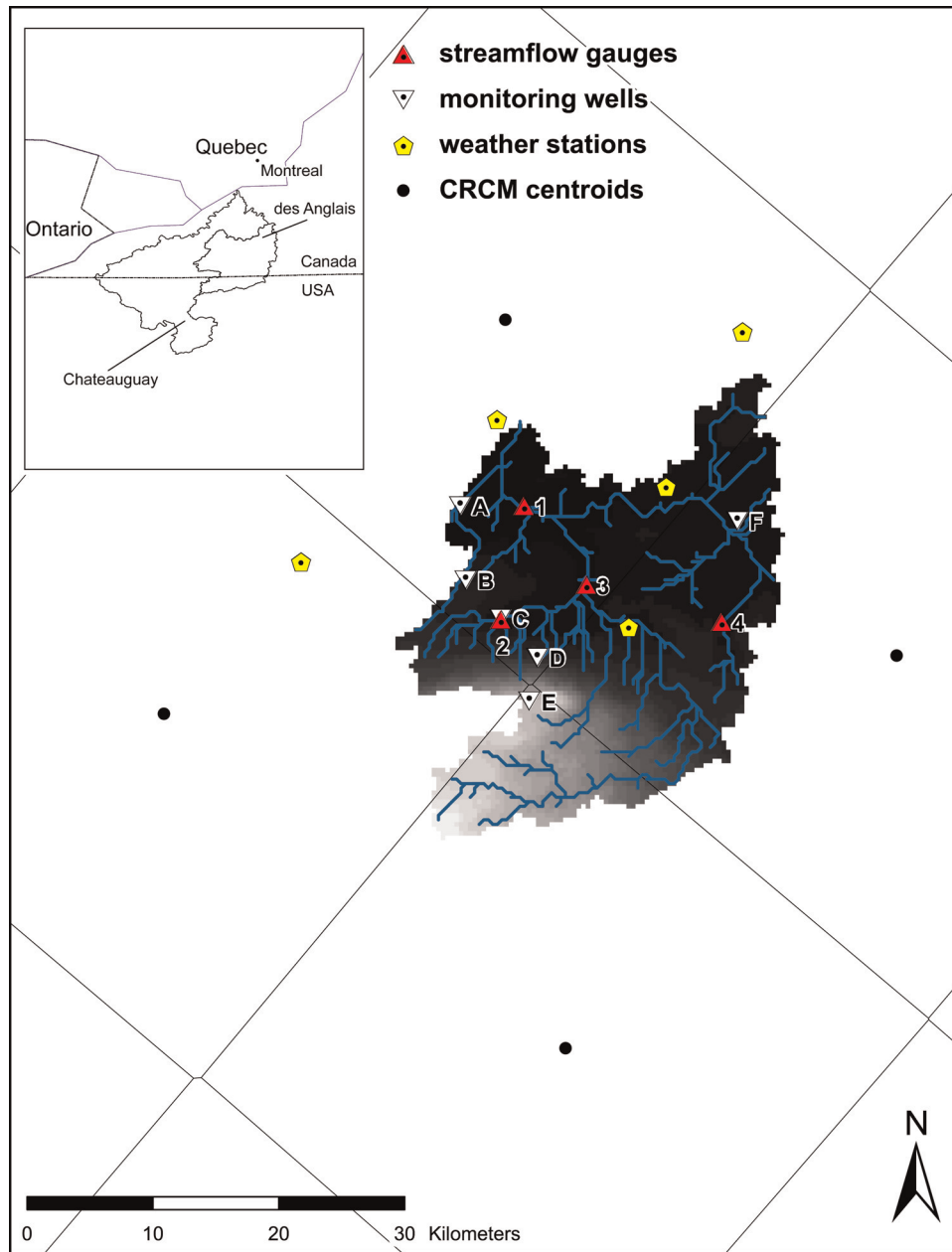


Figure 1. Topographic map of the des Anglais river basin (highest elevations in light gray) showing the network of weather stations, streamflow gauges, and monitoring wells and the centroids of the CRCM grid with their Thiessen polygons. The study area extends from $44^{\circ}48'08''\text{N}$ to $45^{\circ}20'38''\text{N}$ and $73^{\circ}30'10''\text{W}$ to $74^{\circ}06'10''\text{W}$.

3. Simulation Models

3.1. Catchment Hydrological Model

[9] CATHY is a coupled physically based, spatially distributed model for surface-subsurface simulations [Camporose *et al.*, 2010]. The model is based on resolution of a one-dimensional diffusion wave approximation of the Saint-Venant equation for overland and channel routing nested within a solver for the three-dimensional equation for subsurface flow in variably saturated porous media (i.e., Richards equation). The routing scheme derives from a discretization of the kinematic wave equation based on the Muskingum-Cunge, or matched artificial dispersivity, method. Surface

runoff is propagated through a 1-D drainage network of rivulets and channels automatically extracted by a digital elevation model (DEM)-based preprocessor and characterized using hydraulic geometry scaling relationships. The distinction between overland and channel flow regimes is made using threshold-type relationships based on, for instance, upstream drainage area criteria. Lakes and other topographic depressions are identified and specially treated as part of the DEM preprocessing procedure. The subsurface solver is based on Galerkin finite elements in space, a weighted finite difference scheme in time, and linearization via Newton or Picard iteration.

[10] A boundary condition switching procedure is used to partition potential (atmospheric) fluxes into actual fluxes across the land surface and changes in surface storage. This scheme resolves the coupling term in the CATHY equations that represents the interactions between surface and subsurface waters. The switching procedure distinguishes four possible states for a given surface node: ponded, saturated, unsaturated, and air-dry. The distinction between ponded and saturated is based on a threshold parameter that represents the minimum water depth before surface routing can occur (the threshold would be zero, for instance, for perfectly smooth surfaces and higher for increasingly rough surfaces). An air-dry state is the evaporative analog to rainfall saturation in triggering a switch from an atmosphere-controlled process (and a Neumann boundary condition in the model) to a soil-limited stage (and a Dirichlet condition).

3.2. Regional Climate and Land Surface Models

[11] The CRCM is a limited area, three-dimensional, nested grid point atmospheric model based on the fully elastic nonhydrostatic Euler equations [Caya and Laprise, 1999; Music and Caya, 2007]. The equations are solved by noncentered semi-implicit and semi-Lagrangian numerical schemes. The model is run over a regional domain (on typical scales of hundreds to thousands of kilometers) cast on a horizontal grid that is uniform on a polar stereographic projection. A typical horizontal resolution is 45 km. Time-dependent data are provided at the lateral boundaries of the regional domain by reanalyses of observational data or GCM output at coarser horizontal resolutions. The vertical resolution is variable and uses a Gal-Chen scaled terrain following vertical coordinate.

[12] Within the CRCM, turbulent exchanges of energy, water, and momentum at the surface-atmosphere interface are computed by CLASS, a physically based soil-snow-vegetation land surface scheme [Verseghy, 1991; Verseghy et al., 1993]. CLASS is commonly referred to as a second generation scheme (see Pitman [2003] for a comprehensive review) that uses an explicit representation of temperature and liquid and frozen soil moisture for three soil layers (a 10 cm surface layer, a 25 cm vegetation root zone layer, and a 3.75 m deep soil layer), an explicit vegetation canopy allowing stomatal and root zone control of evapotranspiration, and a thermally and hydrologically distinct snowpack present during the cold seasons, acting, in effect, as a fourth separate “soil” layer. For the soil layers, CLASS solves the one-dimensional Darcy equation for vertical fluid flow in porous media (with both suction and gravity terms) and thermal conduction equations for soil temperatures. Water infiltration into the upper soil layer is treated as a downward propagating square wave [Green and Ampt, 1911; Mein and Larson, 1973]. When the infiltration capacity is exceeded, water is considered to be ponded at the surface up to a maximum surface retention capacity, which varies according to land cover, and beyond which surface runoff occurs. Subsurface runoff is crudely simulated as a “bottom drainage” out from the deepest soil layer (0.35–4.10 m depth), parameterized via an empirical power relation linking the saturated hydraulic conductivity and volumetric liquid water content [Clapp and Hornberger, 1978]. As CLASS was meant first and foremost to provide adequate boundary conditions to a coupled atmospheric model

through surface fluxes of water, energy, and momentum, it does not explicitly account for the water table depth, lateral groundwater flow, and surface or subsurface routing to streams, and its soil domain remains within the vadose (unsaturated) zone.

4. Methodology

4.1. Analysis of the Climate Data

[13] Climate projections for past and future conditions were taken from CRCM (version 4.2.3) driven by atmospheric fields from the Canadian General Circulation Model (CGCM, version 3.1), whose atmospheric component is described by Scinocca et al. [2008] and whose ocean and sea ice components and coupling scheme are described by Flato and Boer [2001]. The model run used was ensemble member 3 based on the IPCC Special Report on Emissions Scenario (SRES) A2 [IPCC, 2000]. The simulations were run over the regional domain covering North America (AMNO with 200×192 grid points) with a horizontal grid size mesh of 45 km (polar stereographic projection, true at 60°N). The past CRCM simulation was run over the period 1958–2000 and used the observed greenhouse gas and aerosol concentrations until 2000. The future simulation was run over the period 2038–2070 and used the post-2000 SRES A2 greenhouse gas and aerosol projected evolution [IPCC, 2000]. The same evolutions were used by the driving CGCM. Model output was archived on a 6-hourly basis over the periods considered. The spectral nudging technique [Riette and Caya, 2002] was applied within the interior of the regional domain to keep CRCM’s large-scale flow close to its driving data. Both simulations have a 3 year spin-up period for the climate system to reach equilibrium (the timescale of this equilibrium tends to be dominated by the land surface deep soil layer).

[14] An important issue when considering adaptation and mitigation responses to climate change is the uncertainty in the prediction of future climate [Christensen and Christensen, 2007]. In addition to uncertainty derived from model formulations, there is that derived from natural climate variability and future atmospheric emissions. Thus, the use of data for multiple greenhouse gas emission scenarios from multiple climate models would be beneficial for the definition of an uncertainty envelope of future hydrologic conditions and impacts [Prudhomme et al., 2003; Wilby and Harris, 2006]. As such, the results of the present investigation, performed using a single data set from the CRCM model, can be considered a preliminary analysis of the sensitivity of surface-subsurface interactions to climate change for the considered study area.

[15] The simulated CRCM climate data were analyzed using the nonparametric Mann-Kendall statistical test [Mann, 1945; Kendall, 1975], widely used in hydrological trend detection studies to verify the null hypothesis of no trend in a time series. In this study the test was applied to annual and mean monthly CRCM-generated values for both past and future periods. One problem associated with this test is that the result is affected by serial correlation in the time series. Specifically, if a positive serial correlation is present, the test will suggest a significant trend more often than it actually should [von Storch and Navarra, 1995]. To eliminate this effect without biasing the trend’s

magnitude, we applied the Mann-Kendall test to a prewhitened time series obtained following the procedure proposed by Yue *et al.* [2002], consisting first in removing the slope, then removing the lag 1 serial correlation from the time series, and finally putting back the slope.

[16] The Mann-Kendall test statistic S is given by

$$S = \sum_{k=1}^{n-1} \sum_{j=k+1}^n \text{sgn}(x_j - x_k), \quad (1)$$

where $\text{sgn}(\theta) = 1, 0,$ or -1 for θ positive, zero, or negative, respectively, n is the data set record length, and x_j and x_k are the sequential data values.

[17] The Mann-Kendall test has two parameters that are important for trend detection: the significance level, which indicates the trend's strength, and the slope estimate, which indicates the direction as well as the rate of change. Under the null hypothesis that there is no trend in the data, the distribution of S is expected to have a mean of zero and a variance of $n(n-1)(2n+5)/18$.

[18] The normal Z test statistic is calculated as

$$Z = \begin{cases} \frac{S-1}{\sqrt{\text{var}(S)}} & \text{if } S > 0 \\ 0 & \text{if } S = 0 \\ \frac{S+1}{\sqrt{\text{var}(S)}} & \text{if } S < 0. \end{cases}$$

[19] The null hypothesis is rejected at significance level of α if $|Z| > Z_{(1-\alpha/2)}$, where $Z_{(1-\alpha/2)}$ is the value of the standard normal distribution with a probability of exceedance of $\alpha/2$. A positive value of Z indicates an upward trend, while a negative value represents a downward trend.

[20] Trend magnitude is estimated using a nonparametric median-based slope method proposed by Sen [1968] and extended by Hirsh *et al.* [1982]:

$$\beta = \text{Median} \left[\frac{x_j - x_k}{j - k} \right], k < j, \quad (2)$$

where $1 < k < j < n$. Here β is the median of all possible combinations of pairs for the whole data set.

[21] Statistically significant trends in annual precipitation were not detected for either past or future periods

(Tables 1 and 2). From the analysis of monthly values a significant negative trend was detected for late spring (May) and for two summer months (July and August) of the future period. Positive trends were found in annual mean values of minimum and maximum temperatures for both periods, with a decrease in significance level from 5% to 1% from the past to the future projection. On a monthly basis, only July shows an increasing trend for the past period, for both minimum and maximum temperatures (Table 1). For the future projection most of the calendar months (nine, spread over the four seasons) show significant increasing trends in maximum temperature, while five months (in winter, spring, and summer) do so for minimum temperatures (Table 2).

[22] Overall, the trends detected in the CRCM-generated data for the past period are consistent with the results of a previous study based on an observation data set for the entire country [Zhang *et al.*, 2000], i.e., a statistically significant positive trend found for annual maximum temperatures (and hence in potential evapotranspiration) and almost no statistically significant trend in annual precipitation. In a subsequent analysis of historical streamflow data for Canada, Zhang *et al.* [2001] found that the combination of stable precipitation and increasing temperatures produced a negative trend in annual mean streamflow, an earlier snow and ice melt, and, in addition, an increase in the rainfall proportion of total precipitation. This, in turn, produces more direct runoff and accelerates snowmelt as the wet snowpack absorbs more solar radiation. The consistency with national temperature and precipitation trends for the past period suggests that the CRCM-generated future projection will produce similar changes in streamflow for the des Anglais catchment if directly applied as atmospheric forcing input.

4.2. Hydrological Model Setup

4.2.1. Climate Data

[23] In climate change impact studies, large-scale atmospheric variables need to be related to local- or station-scale meteorological data sets. Scibek and Allen [2006] used a statistical downscaling model to extract monthly change factors from the CGCM and redistribute them to daily time

Table 1. Summary of Trend Analysis for Annual and Monthly Values of Total Precipitation and Maximum and Minimum Temperature for the Past Simulation (1961–1990)^a

	Precipitation			Maximum Temperature			Minimum Temperature		
	Test Z	Significance	Slope β	Test Z	Significance	Slope β	Test Z	Significance	Slope β
Annual	-0.694	ns	-2.350	2.195	**	0.033	2.32	**	0.035
January	-1.369	ns	-0.613	-1.332	ns	-0.091	-0.994	ns	-0.050
February	1.032	ns	0.530	0.844	ns	0.043	1.294	ns	0.093
March	1.144	ns	1.022	1.632	ns	0.063	1.519	ns	0.111
April	0.131	ns	0.124	0.356	ns	0.023	1.294	ns	0.068
May	-0.844	ns	-0.795	0.619	ns	0.033	0.957	ns	0.035
June	-1.632	ns	-0.958	1.444	ns	0.077	0.994	ns	0.029
July	-0.431	ns	-0.326	2.720	***	0.124	2.945	***	0.089
August	-1.482	ns	-1.14	2.444	ns	0.010	0.169	ns	0.006
September	-1.594	ns	-0.685	0.957	ns	0.039	0.469	ns	0.030
October	1.219	ns	0.397	1.219	ns	0.052	0.131	ns	0.009
November	0.694	ns	0.420	0.244	ns	0.008	0.319	ns	0.13
December	0.694	ns	0.427	0.244	ns	0.017	0.994	ns	0.050

^aFor significance, *** and ** indicate significance levels of 0.01 and 0.05, respectively; ns indicates significance level exceeds 0.1.

Table 2. Summary of Trend Analysis for Annual and Monthly Values of Total Precipitation and Maximum and Minimum Temperature for the Future Projection (2041–2070)^a

	Precipitation			Maximum Temperature			Minimum Temperature		
	Test Z	Significance	Slope β	Test Z	Significance	Slope β	Test Z	Significance	Slope β
Annual	-1.519	ns	-3.762	4.033	***	0.094	3.058	***	0.077
January	1.257	ns	0.744	3.170	***	0.161	2.307	**	0.170
February	0.056	ns	0.152	2.795	***	0.189	2.457	**	0.162
March	0.356	ns	0.444	0.732	ns	0.053	1.219	ns	0.112
April	0.019	ns	0.041	2.457	**	0.116	2.908	***	0.139
May	-2.007	**	-1.683	2.682	***	0.123	2.795	***	0.099
June	-0.919	ns	-0.784	2.682	***	0.106	3.020	***	0.083
July	-1.932	*	-1.671	1.707	*	0.107	0.957	ns	0.026
August	-2.908	***	-2.538	2.382	**	0.110	1.632	ns	0.056
September	-1.069	ns	-0.853	1.707	*	0.118	1.294	ns	0.062
October	0.657	ns	0.771	1.932	*	0.083	1.294	ns	0.060
November	0.319	ns	0.226	0.657	ns	0.046	0.994	ns	0.039
December	0.000	ns	0.000	-0.244	ns	-0.013	-0.469	ns	-0.032

^aFor significance, ***, **, and * indicate significance levels of 0.01, 0.05, and 0.1, respectively; ns indicates significance level exceeds 0.1

series using a stochastic weather generator; *van Roosmalen et al.* [2009] applied a monthly deviation between future and past periods to overcome systematic biases in past data between observed and simulated (by a regional climate model) time series; *Chiew et al.* [2009] applied a daily downscaling method that considers changes in future mean seasonal rainfall and daily rainfall distribution to 15 GCM-generated data sets.

[24] For the des Anglais river basin, the CRCM yielded estimates of mean monthly temperature that are comparable to observed data and mean monthly precipitation that vary somewhat from observed values (Figure 2). The observed data shown in Figure 2 cover the same 1961–1990 time period as the CRCM-generated past simulation. Weighted averaging is used to calculate the observed and CRCM data, in the former case using the five weather stations shown in Figure 1 and in the latter case according to the Thiessen polygons, also shown in Figure 1. In Figure 2 we observe, in particular, a marked overestimation of mean precipitation for late spring and summer. To construct the

future climate projection data set for the hydrological model simulations, it was thus necessary to apply a transfer scheme such as the commonly used delta change method [*Hay et al.*, 2000; *van Roosmalen et al.*, 2009], which consists in perturbing baseline meteorological data with monthly change values. The monthly change values are calculated as the difference in CRCM atmospheric outputs between the past and future 30 year climate periods. In applying the delta change method, it is assumed that the relative and/or absolute changes in precipitation and temperature between past and future climate simulations such as simulated by the CRCM have a strong physical basis and that rainfall recurrence patterns remain the same between past and future periods. Thus, scaled and baseline scenarios differ only in terms of their respective means, maxima, and minima; all other properties of the data, such as the range and variability, remain unchanged. The delta change method does not easily apply to precipitation records because the multiplication of observed precipitation by CRCM precipitation changes does not affect the number

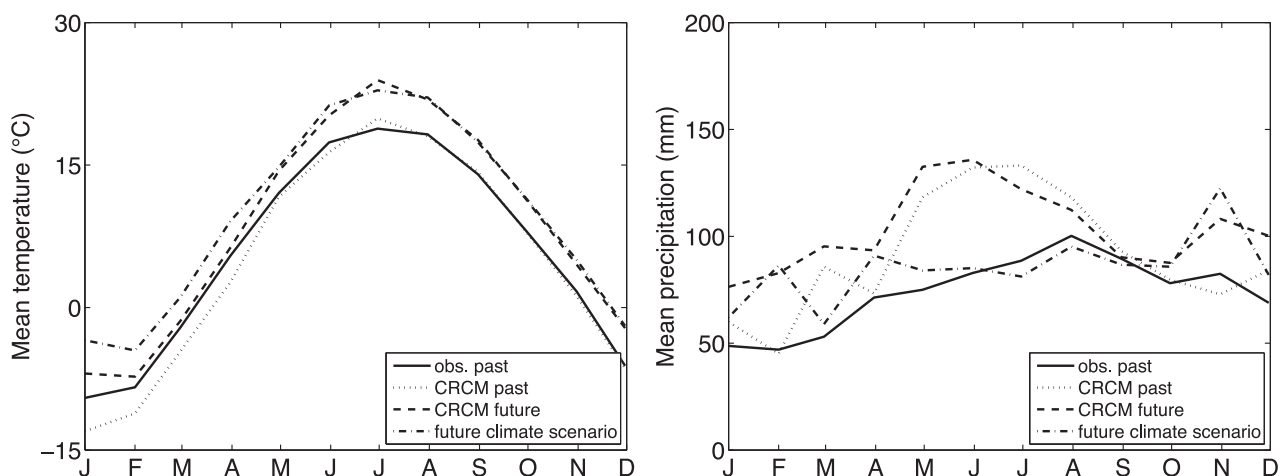


Figure 2. Mean monthly temperature and precipitation: observed past data (solid line), CRCM-generated values for the past simulation (dotted line), CRCM-generated values for the future projection (dashed line), and values for the future climate scenario based on the delta change method (dash-dotted line).

of rain days. This means that the temporal sequencing of wet and dry days is unchanged, and so the method may not be helpful in circumstances where changes in spell lengths are important to the impact assessment. The importance for the des Anglais basin of snow accumulation and snowmelt processes alleviates this limitation to some extent. The CATHY hydrological model was thus driven by the observed 1961–1990 data set (daily precipitation and minimum and maximum temperatures) for the past simulation and by this same baseline data set perturbed as per the delta change method for the future projection.

[25] The precipitation input $P_{\Delta}(i, j, k)$ for day i , month j , and year k of the future projection is calculated as

$$P_{\Delta}(i, j, k) = \Delta_P(j) \times P_{\text{obs}}(i, j, k);$$

$$i = 1, 2, \dots, 31; j = 1, 2, \dots, 12; k = 1, 2, \dots, 30, \quad (3)$$

where P_{obs} is the observed past precipitation and $\Delta_P(j)$ is the delta method correction factor, calculated for each month j as $\overline{P}_f(j)/\overline{P}_p(j)$, where $\overline{P}(j)$ is the mean precipitation for month j averaged over the 30 year CRCM-generated past (p) and future (f) simulations.

[26] In a similar manner, the minimum and maximum temperature inputs are calculated as

$$T_{\Delta}(i, j, k) = \Delta_T(j) + T_{\text{obs}}(i, j, k);$$

$$i = 1, 2, \dots, 31; j = 1, 2, \dots, 12; k = 1, 2, \dots, 30, \quad (4)$$

with the correction factor $\Delta_T(j) = \overline{T}_f(j) - \overline{T}_p(j)$.

[27] The results of applying the delta change method are shown in Figure 2. Compared to the baseline observation data set, mean monthly temperatures increase for all months while mean monthly precipitation increases for all months except July, August, and September. The mean annual temperature for the future projection as corrected by

the delta change method has increased by 3.8°C compared to the baseline case, while the mean annual precipitation has increased by 135 mm, or 15%.

[28] The precipitation and minimum and maximum temperature time series for the observed (1961–1990) and future (2041–2070) climate projections were then used to derive potential evapotranspiration, using the method of *Oudin et al.* [2005], and to reproduce snow accumulation and melting on the basis of the mixed degree-day energy budget method of *Turcotte et al.* [2004]. To account for the main land use classes in the des Anglais catchment (47% agriculture, 37% deciduous forest, and 16% coniferous forest), the snow module was applied using three different values for the snow melting rate (8.37 mm/d $^{\circ}\text{C}$ for agriculture, 7.76 mm/d $^{\circ}\text{C}$ for deciduous forest, and 1.56 mm/d $^{\circ}\text{C}$ for coniferous forest) and for the threshold snow melting temperature (-0.92°C for agriculture, 2.10°C for deciduous forest, and 2.32°C for coniferous forest). These preprocessed time series of potential evapotranspiration and snow-corrected precipitation constitute the final form of the atmospheric input files passed to the CATHY model for simulation of the past and future climate simulations.

4.2.2. Discretization and Parameterization

[29] A 360 m DEM was used to delineate the des Anglais catchment, on the basis of which the 3-D subsurface grid was constructed by subdividing each DEM cell into two triangles and then projecting this 2-D surface mesh vertically for 100 m and 10 layers (the layer thicknesses are given in Table 3). The resulting 3-D grid contains 61,908 nodes and 320,280 tetrahedral elements. The bottom and lateral boundaries of the domain were assumed to be impermeable.

[30] According to calibration trials (described below) and to available pedologic and geologic information [*Lamontagne, 2005; Côté et al., 2006*], different material properties were assigned both vertically and laterally. The four zones shown in Figure 3 represent distinct soil and Quaternary sediment types: the top four layers (0.9 m total

Table 3. Material Properties for the 10 Vertical Layers and Four Geopedologic Zones of the des Anglais Catchment Discretization

	Layer (Top to Bottom)									
	1	2	3	4	5	6	7	8	9	10
Layer thickness (m)	0.05	0.1	0.3	0.45	1.10	2.10	5.90	20	30	40
Zone 1										
K_h (m/s)	5×10^{-4}	5×10^{-4}	5×10^{-4}	5×10^{-4}	1×10^{-4}	5×10^{-9}	5×10^{-9}	1×10^{-7}	5×10^{-8}	5×10^{-8}
K_z (m/s)	3×10^{-4}	3×10^{-4}	3×10^{-4}	3×10^{-4}	5×10^{-4}	3×10^{-9}	3×10^{-9}	5×10^{-7}	5×10^{-8}	5×10^{-8}
θ_s	0.5	0.5	0.5	0.5	0.4	0.5	0.5	0.5	0.1	0.1
S_s (m^{-1})	5×10^{-4}	5×10^{-4}	5×10^{-4}	5×10^{-4}	1×10^{-4}	5×10^{-9}	5×10^{-9}	1×10^{-7}	5×10^{-8}	5×10^{-8}
Zone 2										
K_h (m/s)	5×10^{-4}	5×10^{-4}	5×10^{-4}	5×10^{-4}	1×10^{-5}	1×10^{-5}	1×10^{-7}	5×10^{-8}	5×10^{-8}	5×10^{-8}
K_z (m/s)	3×10^{-4}	3×10^{-4}	3×10^{-4}	3×10^{-4}	5×10^{-5}	5×10^{-5}	5×10^{-7}	5×10^{-8}	5×10^{-8}	5×10^{-8}
θ_s	0.5	0.5	0.5	0.5	0.5	0.5	0.5	0.1	0.1	0.1
S_s (m^{-1})	1×10^{-5}	1×10^{-5}	1×10^{-5}	1×10^{-5}	1×10^{-4}	1×10^{-4}	1×10^{-4}	1×10^{-6}	1×10^{-6}	1×10^{-6}
Zone 3										
K_h (m/s)	5×10^{-4}	5×10^{-4}	5×10^{-4}	5×10^{-4}	1×10^{-4}	1×10^{-4}	2×10^{-6}	2×10^{-6}	2×10^{-6}	2×10^{-6}
K_z (m/s)	3×10^{-4}	3×10^{-4}	3×10^{-4}	3×10^{-4}	5×10^{-4}	5×10^{-4}	5×10^{-8}	5×10^{-8}	5×10^{-8}	5×10^{-8}
θ_s	0.5	0.5	0.5	0.5	0.4	0.4	0.1	0.1	0.1	0.1
S_s (m^{-1})	1×10^{-5}	1×10^{-5}	1×10^{-5}	1×10^{-5}	1×10^{-4}	1×10^{-4}	1×10^{-6}	1×10^{-6}	1×10^{-6}	1×10^{-6}
Zone 4										
K_h (m/s)	5×10^{-8}	5×10^{-8}	5×10^{-8}	5×10^{-8}	1×10^{-7}	1×10^{-7}	1×10^{-7}	5×10^{-8}	5×10^{-8}	5×10^{-8}
K_z (m/s)	3×10^{-8}	3×10^{-8}	3×10^{-8}	3×10^{-8}	5×10^{-7}	5×10^{-7}	5×10^{-7}	5×10^{-8}	5×10^{-8}	5×10^{-8}
θ_s	0.9	0.9	0.9	0.9	0.5	0.5	0.5	0.1	0.1	0.1
S_s (m^{-1})	1×10^{-5}	1×10^{-5}	1×10^{-5}	1×10^{-5}	1×10^{-4}	1×10^{-4}	1×10^{-4}	1×10^{-6}	1×10^{-6}	1×10^{-6}

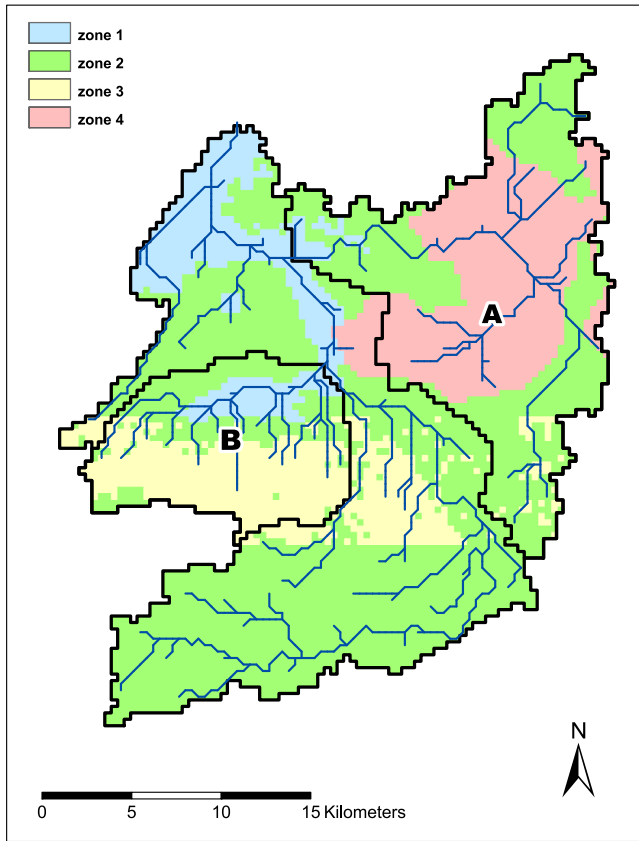


Figure 3. Map of the des Anglais watershed with four geopedologic zones and two subcatchments: A, Norton, and B, Rivière Noire.

thickness) are a loamy sand for zones 1, 2, and 3 and an organic soil for zone 4; the next layers are Quaternary stratigraphic sequences of fluviglacial coarse sand–marine clay and fine silt–till–bedrock for zone 1, reworked till–till–bedrock for zone 2, fluviglacial coarse sand–bedrock for zone 3, and till–bedrock for zone 4. Table 3 summarizes the saturated hydraulic conductivity (K_h , K_z), porosity (θ_s), and specific storage (S_s) attributed to each zone and layer of the discretized domain. A high degree of anisotropy (two orders of magnitude) was attributed to the bottom four layers in zone 3 following indications of preferential horizontal flow paths in this region of the fractured bedrock aquifer [Côté *et al.*, 2006]. Zone 3 includes Covey Hill, an elongated (east–west) plateau that is the most pronounced topographic feature in the Canadian part of the des Anglais river basin. The soil hydraulic properties were described by the *van Genuchten and Nielsen* [1985] relationships with residual moisture content $\theta_{res} = 0.07$, air entry pressure head $\psi_a = -0.2$ m, and fitting exponent $n = 2.0$.

[31] The conditions of regional groundwater flow in the bedrock aquifer system were assessed on the basis of the physical properties of the unconsolidated sediments and their corresponding thicknesses. Confined flow prevails where more than 5 m of fine marine sediments with low hydraulic conductivity are present (zone 1 in Figure 3, representing about 10% of the catchment area, and layers 6 and 7 in Table 3). Semiconfined flow conditions are present in areas characterized by fine marine sediments of less than

5 m thickness or by at least 3 m of till (75% of the catchment, zones 2 and 4). Finally, areas with rock outcropping or where the bedrock is covered by less than 3 m of till or by permeable sediments, regardless of their thickness, were designated as unconfined water table aquifers (15% of the catchment, zone 3).

[32] The channel network was identified from the DEM of the catchment using an upstream drainage area threshold of 2.0 km² on the basis of visual similarity between the extracted network and the streamlines depicted on topographic maps. Structural parameters for the channel and overland flow networks were calibrated using, for channel dynamics, the bankfull discharge measured at the main streamflow station (gauge 1 in Figure 1) as a reference value for the flow rate and, for overland (rivulet flow) dynamics, values reported in literature studies as a basis [Emmett, 1978; Bathurst, 1986, 1993; Abrahams *et al.*, 1994]. The values obtained are reported in Table 4.

4.3. Hydrological Model Calibration

[33] As mentioned, the CATHY model was calibrated for subsurface hydraulic conductivity (Table 3) and surface hydraulic geometry (Table 4) parameters. The observation data used was daily streamflow close to the outlet of the catchment (gauge 1 in Figure 1), and the simulation period was 12 months, from October 2001 to October 2002. The parameterization was then verified for a 39 month simulation (October 2002 to January 2006) against daily streamflow at the outlet, for a 5 month simulation (August 2005 to January 2006) against daily streamflow at three internal stations (gauges 2, 3, and 4 in Figure 1), and for a 12 month simulation (May 2004 to May 2005) against daily groundwater level data at the six monitoring wells shown in Figure 1. We present here only the final results of the calibration and verification exercises. A detailed sensitivity study of the CATHY model with tests conducted on the des Anglais catchment is reported by *Sulis et al.* [2010].

[34] Model performance was measured using the root-mean-square error (RMS) for groundwater head and the RMS, the Nash-Sutcliffe efficiency coefficient E , and the percentage error in peak (PEP) for stream discharge [Nash and Sutcliffe, 1970; Anderson and Woessner, 1992; Jones *et al.*, 2008]:

$$E = 1 - \frac{\sum_{i=1}^n (\Omega_{obs,i} - \Omega_{sim,i})^2}{\sum_{i=1}^n (\Omega_{obs,i} - \bar{\Omega}_{obs})^2}, \quad (5)$$

Table 4. Hydraulic Geometry Parameters for the Surface Routing Module of the Hydrological Model

Parameter ^a	Hillslope Cells	Channel Cells
Reference drainage area A_s (m ²)	1.2×10^6	690×10^6
Reference discharge Q_f (m ³ /s)	1	100
Water surface width $W(A_s, Q_f)$ (m)	1	50
Gauckler-Strickler conductance coefficient k_s (m ^{1/3} /s)	0.5	18
“At-a-station” scaling exponents [a], [b], b', and y'	0.36, 0	0.26, 0
“Downstream” scaling exponents [a], [b], b'', and y''	0.5, 0	0.5, 0

^aFor [a], $W(A, Q) = W(A_s, Q_f) Q_f (A/A_s)^{-b'} (A/A_s)^{(b''-b')} Q^{b'}$ For [b], $k_s(A, Q) = k_s (A_s, Q_f) Q_f (A/A_s)^{-y'} (A/A_s)^{(y''-y')} Q^{y'}$

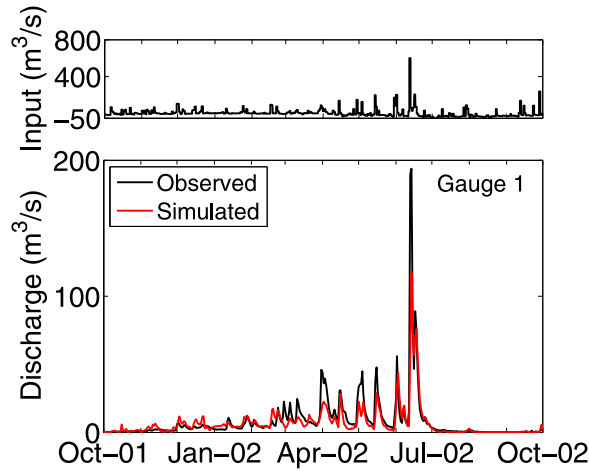


Figure 4. Observed (black line) and simulated (red line) discharge for the calibration period at the main streamflow gauge of the catchment.

$$\text{RMS} = \sqrt{\frac{1}{n} \sum_{i=1}^n (\Omega_{\text{obs},i} - \Omega_{\text{sim},i})^2}, \quad (6)$$

$$\text{PEP}_j = \left[\frac{\max(\Omega_{\text{obs},j}) - \max(\Omega_{\text{sim},j})}{\max(\Omega_{\text{obs},j})} \right] \times 100; \quad j = 1, \dots, m, \quad (7)$$

where Ω_{obs} , Ω_{sim} and $\overline{\Omega_{\text{obs}}}$ are the observed, simulated, and average observed state variables (head, discharge, and peak discharge), n is the number of observations, and m is the number of discharge events manually extracted for estimation of PEP. $E = 1$ when there is a perfect match between simulated and observed values and is negative when the simulation is worse at capturing the observations than the mean value of the observed data. Values of RMS and PEP are zero when the match is perfect and increase as the discrepancy between simulation and observation increases.

[35] Figure 4 shows the simulated and observed hydrographs at the main gauging station for the calibration run, which produced performance measures of $E = 0.70$, $\text{RMS} = 9.7 \text{ m}^3/\text{s}$ for a mean observed discharge of $6.6 \text{ m}^3/\text{s}$, and

an average PEP of 10% (underestimation), with a maximum of 39% reached for the event of 10–16 June 2002. Despite some disagreements in the peaks, the model captures the dynamics of the catchment quite well in both the rising and recession portions of the hydrograph. The good performance of the model was confirmed for the verification tests (Figures 5 and 6), where an efficiency index of $E = 0.69$ and an RMS value of $7.1 \text{ m}^3/\text{s}$ resulted for the main streamflow gauge, and reasonable measures were also obtained at the internal streamflow stations ($E = 0.55$ and $\text{RMS} = 0.74 \text{ m}^3/\text{s}$ for gauge 2, $E = 0.6$ and $\text{RMS} = 3.9 \text{ m}^3/\text{s}$ for gauge 3, and $E = 0.7$ and $\text{RMS} = 0.52 \text{ m}^3/\text{s}$ for gauge 4) and at the monitoring wells. In terms of peak flow errors, the average and maximum PEP values for the verification runs were 3% and 70%, respectively, at the main outlet and 25% and 70%, 3% and 90%, and 13% and 56% at internal gauges 2, 3, and 4, respectively. The high PEP values obtained in the calibration and verification tests, with a prevalence of a negative bias, i.e., underestimation of peak discharges, can probably be attributed to uncertainty in the hydraulic parameters for the overland routing module, in particular, the Gauckler-Strickler coefficient, which were estimated on the basis of literature values, as already mentioned. Indeed, the higher PEP values at the internal gauges are consistent with this hypothesis since at smaller scales, overland flow can become more prevalent in the overall hydrologic response of a catchment to storm events.

[36] For the six well hydrographs (Figure 6) the RMS values ranged from 0.3 to 4.3 m, with the largest value occurring at the well located on the foothill of Covey Hill (well D in Figure 1), where the observed groundwater depth is about 6 m below ground surface. Although the RMS values are reasonable and the graphs in Figure 6 show that the model reproduces groundwater fluctuations reasonably well, it can also be seen that the simulated fluctuations are somewhat dampened for the deeper wells. This is probably due to the use of a coarser mesh in the model for the deeper layers (see Table 3), which diminishes the ability to capture local heterogeneities and fluctuations. It is also apparent in Figure 6 that there is systematic overprediction of groundwater levels, most probably attributable to a combination of the no-flow boundary condition assigned to the lateral

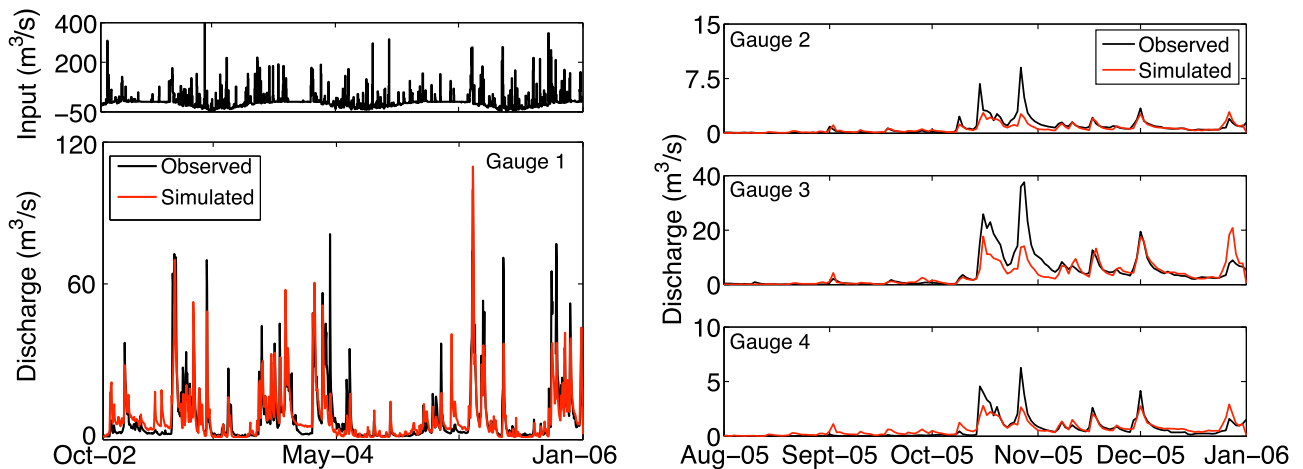


Figure 5. Observed (black line) and simulated (red line) discharge at the four gauges of the catchment for the verification period.

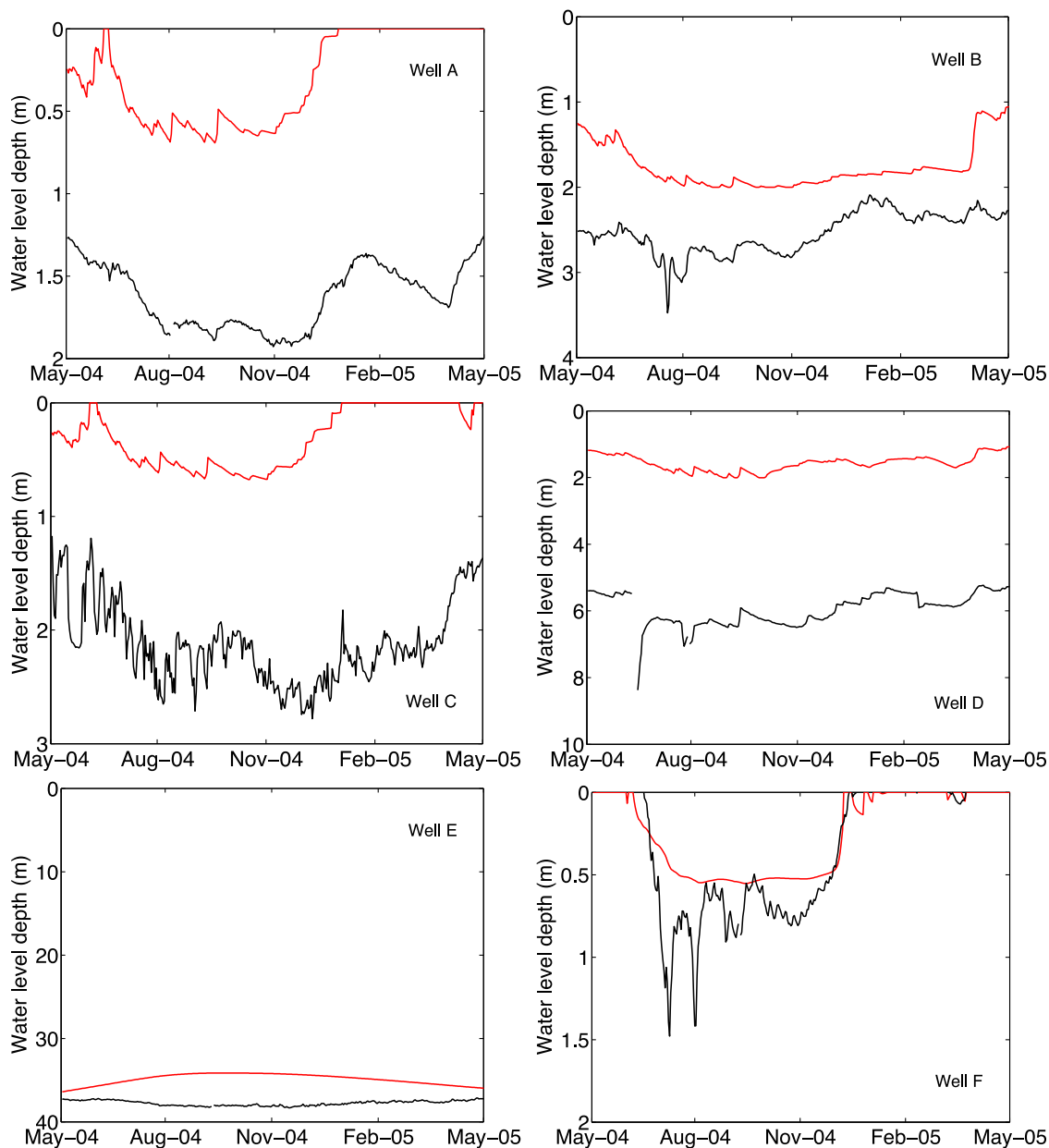


Figure 6. Observed (black line) and simulated (red line) water table depths at the six monitoring wells for the verification period.

boundaries of the subsurface domain, preventing regional (interbasin) groundwater flow, and the fact that no other outflow boundaries (e.g., seepage faces along incised stream banks) were assigned that could maintain water tables at a lower level. All subsurface water exits the catchment at the surface, as overland or channel flow and as evaporation. In the absence of field data to support accurate implementation of internal or lateral outflow boundaries, it was preferred to keep the model setup as simple as possible.

5. Simulations

[37] The potential climate change impacts at the des Anglais river basin were assessed by running the calibrated CATHY model with the observed past atmospheric data set and with the hypothetical future data set obtained through

the delta change transfer method. The assessment examines in particular the impacts on river discharge, aquifer recharge, and near-surface soil water storage. The fully coupled, distributed model is used to highlight the role played by feedback processes between the surface and subsurface and the influence of factors such as topography and heterogeneity. An additional set of simulations was performed, using directly the CRCM-generated past and future scenarios, to compare the CATHY and CLASS models in terms of surface and subsurface runoff and soil water storage.

5.1. Climate Change Impacts

5.1.1. River Discharge

[38] The sensitivity of river discharge to the changing atmospheric input was evaluated at the catchment outlet

and at the outlet of two subcatchments having different physiographic features (the Norton and Rivière Noire subcatchments in Figure 3). The Norton subcatchment, with a relatively flat topography, low-permeability organic soils, and semiconfined aquifer conditions, represents a case of weak interactions between surface and subsurface water, while the Rivière Noire, which includes Covey Hill, rock outcrops, and a fractured bedrock aquifer under unconfined conditions, is an area where we expect significant surface and subsurface interactions. Daily discharge values at the three outlets were averaged to obtain mean monthly values over the 1961–1990 and 2041–2070 periods. Mean monthly discharge ratios (future over past) were then calculated and plotted in Figure 7.

[39] At the main outlet of the des Anglais catchment the climate change impacts are more significant during the peak winter (January–February) and summer (July–August) months, with a strong increase in future discharge in winter and a strong decrease in summer. The winter effect is due to the combination of more precipitation and higher temperatures, which increases the proportion of rainfall to snowfall. Higher temperatures also lead to a reduction in snow cover, resulting in a shift in spring freshet from April to March and a decrease in streamflow during the spring season. In the summer, the strong decrease in river discharge is the result of a slight decrease in total precipitation combined with a marked increase in evaporation due to higher temperatures. The watershed's response to increased precipitation in the fall for the future scenario is delayed (to late November) because of the storage deficit that developed in the basin over the summer period, resulting in more infiltration and recharge and less runoff in early fall.

[40] The impacts on the two subcatchments generally follow the same trend detected at the main outlet, although marked differences in sensitivity to the changing climate can be observed in Figure 7 owing to a different partitioning between the overland runoff and base flow components of the hydrograph. For the Rivière Noire subcatchment, the

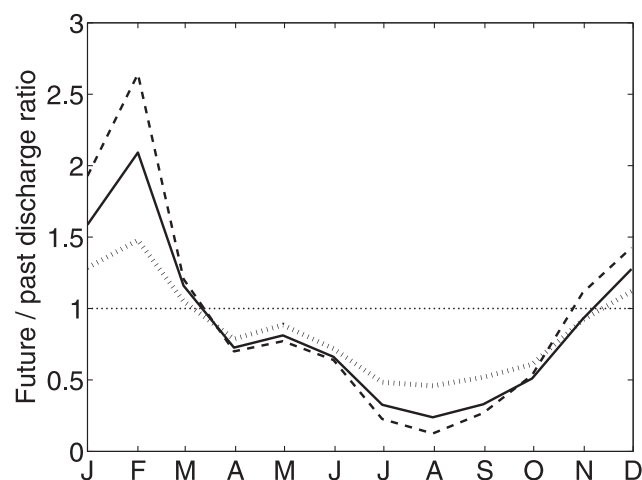


Figure 7. Ratio of mean monthly discharge simulated under future climate conditions to mean monthly discharge simulated under the past climate: des Anglais catchment outlet (solid line), Norton subcatchment outlet (dashed line), and Rivière Noire subcatchment (dotted line).

decrease in river discharge during the summer period is alleviated by a greater base flow component as a result of the larger amount of water infiltrated in early spring. The Norton subcatchment, on the other hand, with its less permeable soils and weaker surface-subsurface connections, has a dominant overland flow component, resulting in a faster and sharper response to the forcing climate. This higher sensitivity is seen in Figure 7 in both the peak winter discharge increase and the peak summer low-flow period. The results at the different outlets indicate how local heterogeneity in topography, soils, and geology can result in significant spatiotemporal variations in a catchment's response to climate change.

5.1.2. Recharge to the Aquifer

[41] Recharge is computed in the CATHY model as the downward flux of water across the water table. Daily nodal recharge values were spatially cumulated and temporally averaged to obtain mean monthly values for the past and future periods, and the future/past ratio was then calculated and plotted in Figure 8. The aquifer of the des Anglais basin receives most of its recharge in the spring and fall through snowmelt and heavier rainfall, respectively. In agreement with other studies [Eckhardt and Ulbrich, 2003; Toews and Allen, 2009], Figure 8 shows that climate change for the des Anglais results in a significant increase in winter season recharge due to a higher rain/snow ratio caused by higher temperatures, less recharge in the spring due to an earlier and less intense snowmelt, a general decrease over the summer due to increased evaporation, and an increase in the fall due to increased precipitation. The important role of surface-subsurface interactions is evident in comparing the fall response for recharge (Figure 8) and for streamflow (Figure 7); the aquifer responds quickly to the increased precipitation, contributing to the lag in discharge response mentioned in section 5.1.1.

[42] Figure 9 shows the spatial distribution of the difference in mean monthly aquifer recharge between the future and past climate simulations. General spatial and intra-annual patterns are clearly observable and are consistent

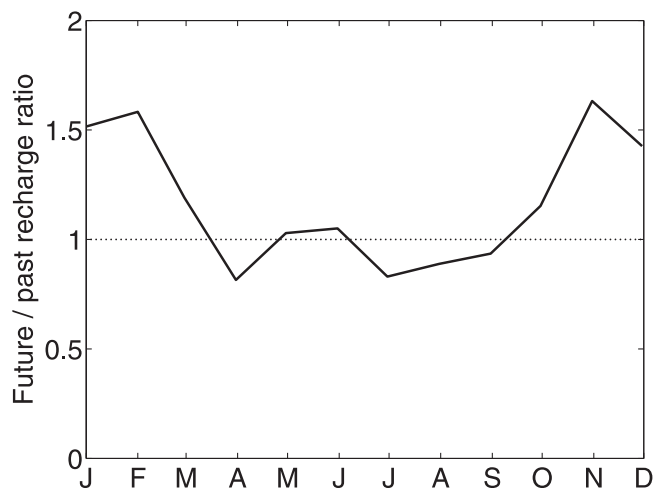


Figure 8. Ratio of mean monthly total recharge simulated under future climate conditions to mean monthly total recharge simulated under the past climate.

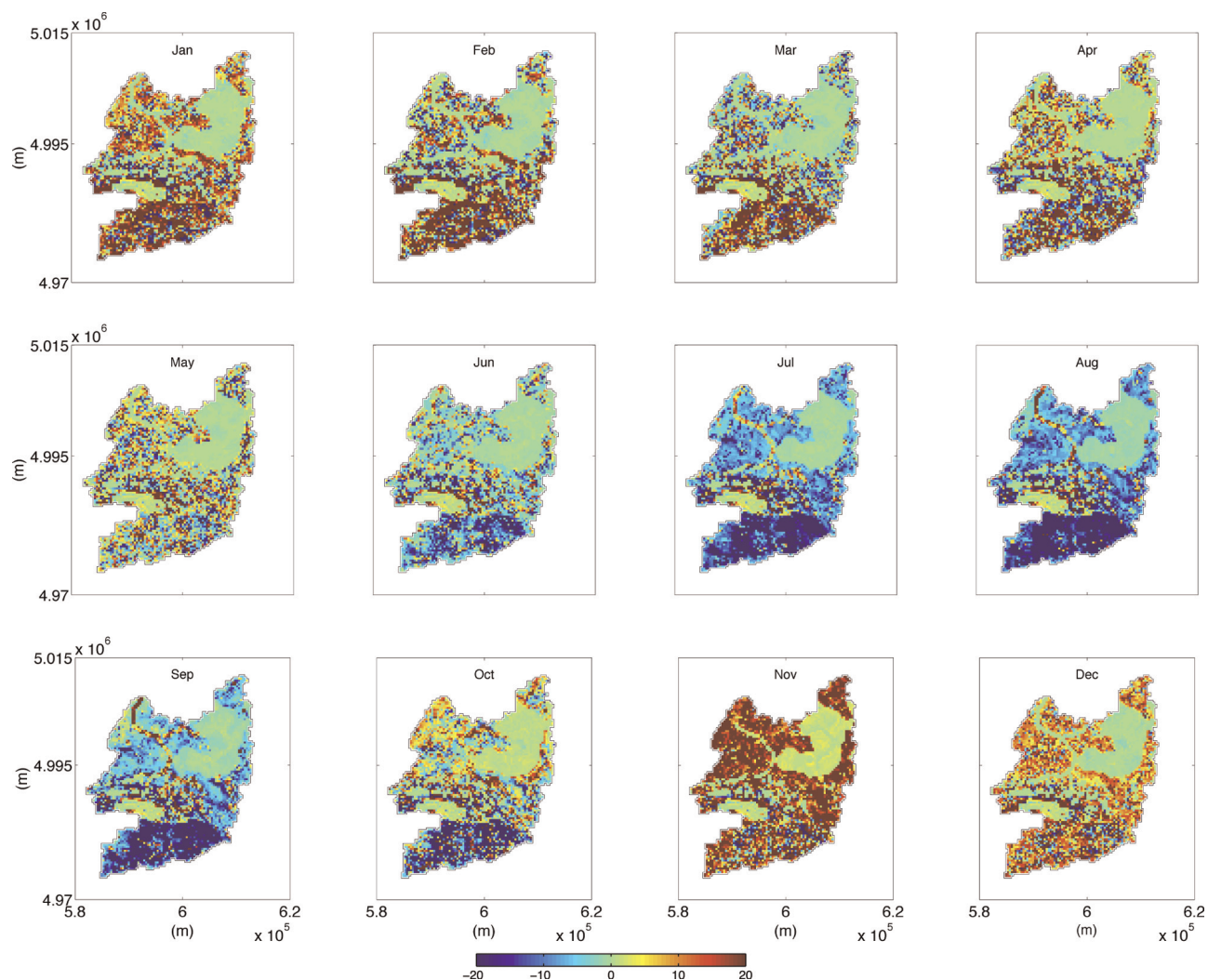


Figure 9. Distributed difference (mm) between mean monthly recharge simulated under future climate conditions and mean monthly recharge simulated under the past climate.

with what was observed for the entire catchment, even though at the fine scale, there are regions that show some strong variability from cell to cell, in particular, in and around zones 1 and 3, where there are pockets of heterogeneity (from zone 2 cells), and in the southern portion of the catchment, where the deeper water table lies within thicker grid layers. These factors can cause numerical difficulties (e.g., oscillations) in the subsurface flow solver. Figure 9 shows an increase in future recharge in the winter and fall periods and a decrease in the summer. Zones 3 and 4 are the least sensitive to climate change in terms of recharge because of the low aquifer porosity and high anisotropy in zone 3 and the low-permeability soils and aquifer in zone 4. The strongest response, throughout the year, is obtained for the southern portion of the catchment, where elevations are highest. Recharge along the main branch of the des Anglais river, discernible throughout the year in Figure 9, remains relatively insensitive to climate change, indicating that the river continues to be fed by the groundwater reservoir. However, during the summer months (July–September), there are occurrences of a large positive change in recharge along this main branch of the channel network,

suggesting a possible reversal in groundwater–river interaction in response to a groundwater storage deficit.

5.1.3. Soil Water Storage

[43] The sensitivity of soil water storage to climate change was evaluated at the surface (top 5 cm) and at different soil depths (0.15, 0.45, 0.90, and 2.0 m). The daily values simulated at each node of the domain were averaged to obtain both aggregated and distributed mean monthly values for the catchment. The relative variation between past and future climate simulations for the entire catchment was assessed by computing an index ratio as in the previous analyses, and the results are plotted in Figure 10. Compared to water fluxes across a point or boundary (discharge at a catchment outlet in Figure 7 and recharge across the water table in Figure 8), water storage volumes are apparently less sensitive to climate change. The changes from past to future climate shown in Figure 10 are most strongly felt nearest to the surface, which is directly exposed to variations in precipitation and evapotranspiration and are progressively dampened as soil depth increases. In terms of intra-annual dynamics, the patterns are nonetheless similar to those observed for recharge and discharge, with all soil

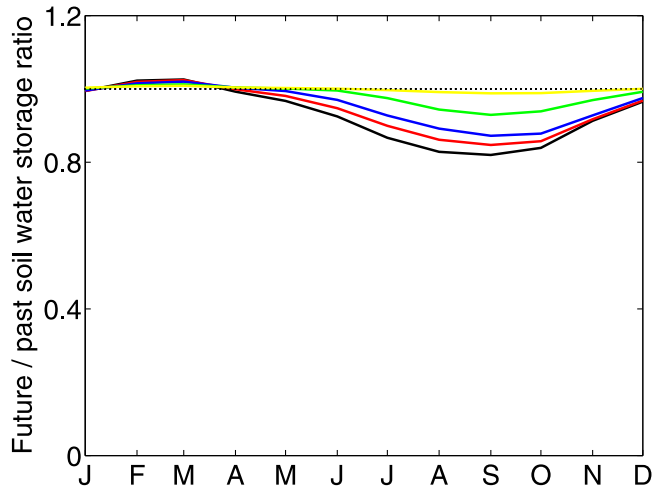


Figure 10. Ratio of mean monthly soil water storage simulated under future climate conditions to mean monthly soil water storage simulated under the past climate: 0.05 m depth (black line), 0.15 m depth (red line), 0.45 m depth (blue line), 0.90 m depth (green line), and 2.0 m depth (yellow line).

depths displaying a decrease in subsurface storage during the summer period and an increase (albeit very slight) over the peak winter and early spring months.

[44] For the top layer of the model discretization (0–5 cm), the future/past soil water ratio computed above was also examined spatially. From a visual analysis of the plots in Figure 11 we can observe a spatial organization of soil moisture variability that follows the topographic and pedologic characteristics (heterogeneity) of the catchment [Western *et al.*, 1999]. In particular, the effect of a lateral redistribution of water is evident in the persistence of the main river network, discernible through most the year. The influence of the greater holding capacity (porosity of 0.90) of the organic soils in zone 4 can also be seen in the faster near-surface response of this region of the catchment in losing water under stress periods and regaining water under wetter conditions. In Figure 11 we can also discern a difference in hydrologic response between regions of the catchment where the exfiltration process during dry periods quickly becomes soil limited because of a deeper water table (for example Covey Hill) and areas with a shallower water table where exfiltration remains predominantly atmosphere controlled. In the latter areas more water is lost during the dry summer period, resulting in a greater soil moisture deficit compared to Covey Hill, and this deficit therefore persists longer into the fall, when there is a return to wetter conditions.

[45] To further explore the role of topography in describing the sensitivity of soil moisture to climate change, we investigated the relationship between the tangent curvature of the surface, as defined by Mitasova and Hofierka [1993], and the mean monthly surface soil water ratio calculated earlier. This analysis was performed for the inset area depicted in Figure 11, which demonstrates a varied response to climate change. Figure 12 shows the scatterplots between the tangent curvature of the surface and the monthly moisture, with the overland (hillslope) and chan-

nel cells plotted separately. It can be seen that there is a strong seasonal variation in the relationship between surface soil moisture and tangent curvature and that this relationship is quite different between hillslope cells and channel cells. We found, for instance, that the hillslope cells having a negative curvature (and thus located along convergent parts of the catchment) are those that tend to experience an increase in soil moisture content for February and March in response to climate change and less variation in the late summer and early fall (August to October). The correlation between the sensitivity of surface soil water content to climate change and the tangent curvature was quite weak for the other months of the year, when near-surface moisture variations are probably more controlled by factors such as evapotranspiration rather than lateral redistribution of water. The correlation was equally weak for channel cells, throughout the year, probably because of the conditions of saturation or near saturation that characterize these cells.

5.2. Comparison With the CLASS Model

[46] As major components of the water cycle, surface and subsurface runoff and soil water storage play a critical role in the global and regional climate system. Many different models, operating over a range of scales from small field plots to continents, are used to simulate these and other hydrological processes. Climate models are continually evolving in terms of their spatial resolution and their parameterization of soil and groundwater flow components, while detailed process-based hydrological models are being increasingly used beyond the hillslope and subcatchment scale. These two classes of models are still far from any sort of convergence toward a unified hydroclimatological simulation paradigm, and it can be instructive to compare their formulations or predictive capabilities when opportunities to do so arise.

[47] The CRCM model (using CLASS internally coupled to its atmospheric part) was used to provide predictions of runoff and soil water storage for the past and future climate simulations at the CRCM grid scale, for the four grid points shown in Figure 1. With appropriate averaging to ensure consistency, these outputs were compared to results produced by CATHY over the des Anglais river basin and at its outlet. The actual CRCM-generated data were used (for the periods 1961–1990 and 2041–2070) instead of the observed past and delta change-generated future data. In this way, both CLASS and CATHY are forced by the same precipitation input. For the actual evaporation, CLASS performs an energy balance at the ground surface, while CATHY uses a threshold value of pressure head ψ_{\min} that corresponds to the advent of stage two evaporation [Salvucci, 1997]. The soil layer saturated hydraulic conductivity K_z and saturated porosity θ_s used in CLASS are related to soil texture information (percent sand) via empirical relationships presented by Cosby *et al.* [1984], while bedrock depth is assigned for each CRCM grid point (Table 5). Moreover, for each of these grid points, four vegetation groups (needleleaf trees, broadleaf trees, crops, and grass) and urban areas are considered in CLASS. This information is obtained by making use of the global archive of Wilson and Henderson-Sellers [1985], which contains listings of primary and secondary land covers at a resolution of $1^\circ \times 1^\circ$.

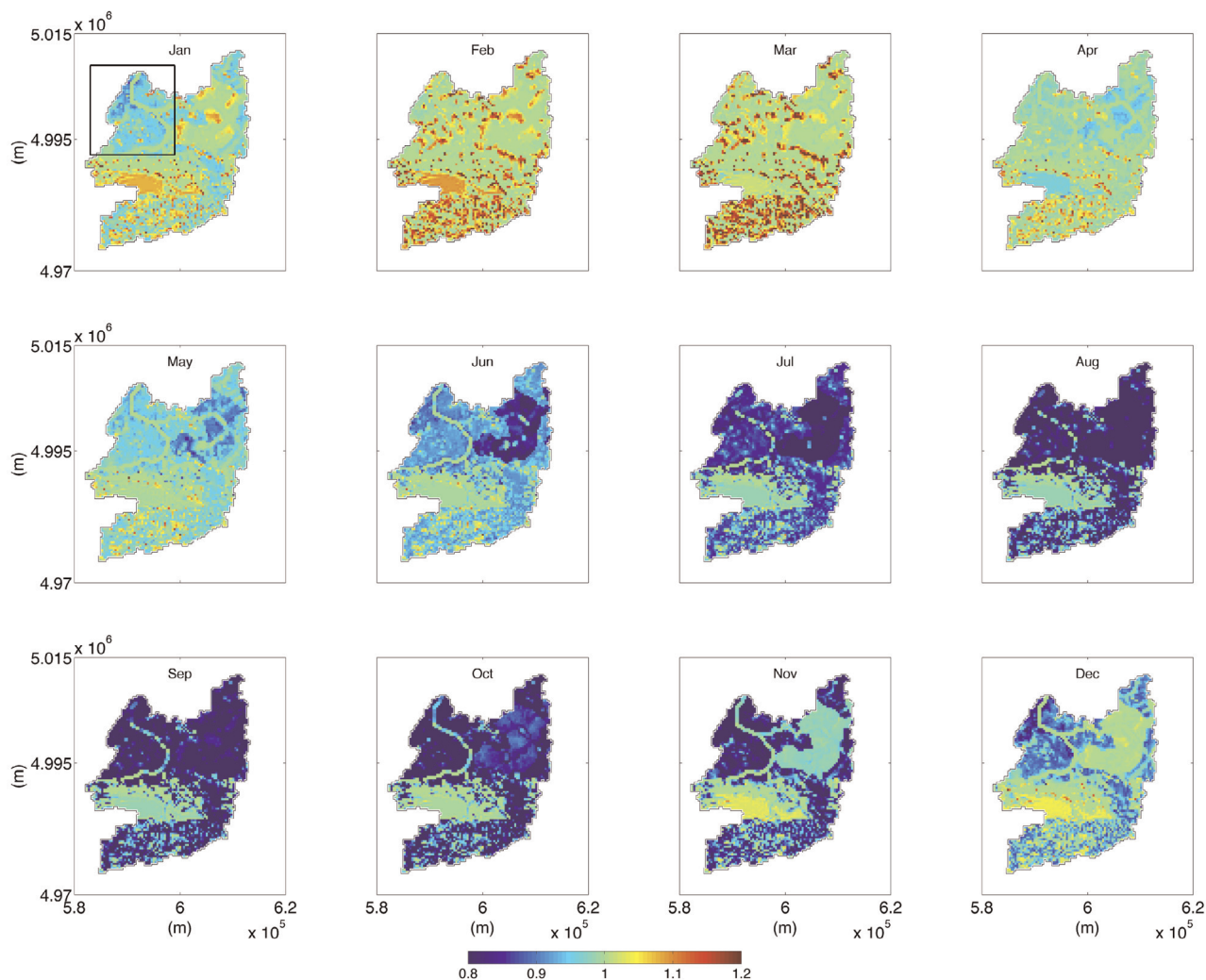


Figure 11. Distributed ratio of mean monthly surface soil moisture (5 cm depth) simulated under future climate conditions to mean monthly surface soil moisture simulated under the past climate.

The vegetation parameters considered are the fractional areal coverage (FCAN), the visible and near-infrared albedo (ALVC and ALIC), the vegetation roughness length in logarithmic scale (LNZ0), the maximum and minimum leaf area index (LAMX and LAMN), the canopy mass (CMAS), and the root depth (ROOT). The set of values used is reported in Table 6, while further details on the way CLASS is parameterized are provided by *Verseghy et al.* [1993].

[48] In order to compare to the CRCM and CLASS simulations, CATHY was rerun using values for soil hydraulic properties, soil texture, and vertical discretization that are consistent with those in CLASS. In particular, CATHY's soil parameters for each Thiessen polygon (Figure 1) were set to the values used in CLASS (Table 5), while the bedrock aquifer was simulated by assigning a much lower hydraulic conductivity (5×10^{-8} m/s), as well as lower porosity and specific storage, to the layers below CLASS's bedrock depth. The CATHY parameterization is summarized in Table 7. As can be seen in Table 7, CATHY's layers 1 and 2 were assigned CLASS's layer 1, CATHY's layers 3 and 4 were assigned CLASS's layer 2, and

CATHY's layers 5–8 were assigned CLASS's layer 3. CATHY's remaining layers 9–12 (beyond a depth of 4.1 m) are not part of CLASS's soil profile. Also, we can see that CATHY's bedrock starts at layer 8 (depth of 3 m) for CRCM grid points 1 and 2, at layer 7 (depth of 1.7 m) for grid point 3, and at layer 6 (depth of 1.2 m) for grid point 4.

5.2.1. Surface and Subsurface Runoff

[49] The sum of surface and subsurface runoff simulated by CLASS at each CRCM grid point was spatially averaged according to the Thiessen polygons shown in Figure 1 and compared with the river discharge simulated by CATHY at the main outlet of the des Anglais catchment. The mean monthly values of this runoff and streamflow are shown in Figure 13 for the 1961–1990 and 2041–2170 periods. For reference (and mindful of the discrepancies between the observed and CRCM-generated data sets discussed earlier; see Figure 2), we also show, for the past period in Figure 13, the mean monthly streamflow observed over the period 1961–1990 and the CATHY results over this same period using the calibration described in section 4.3. It is important to note that the calibration procedure for

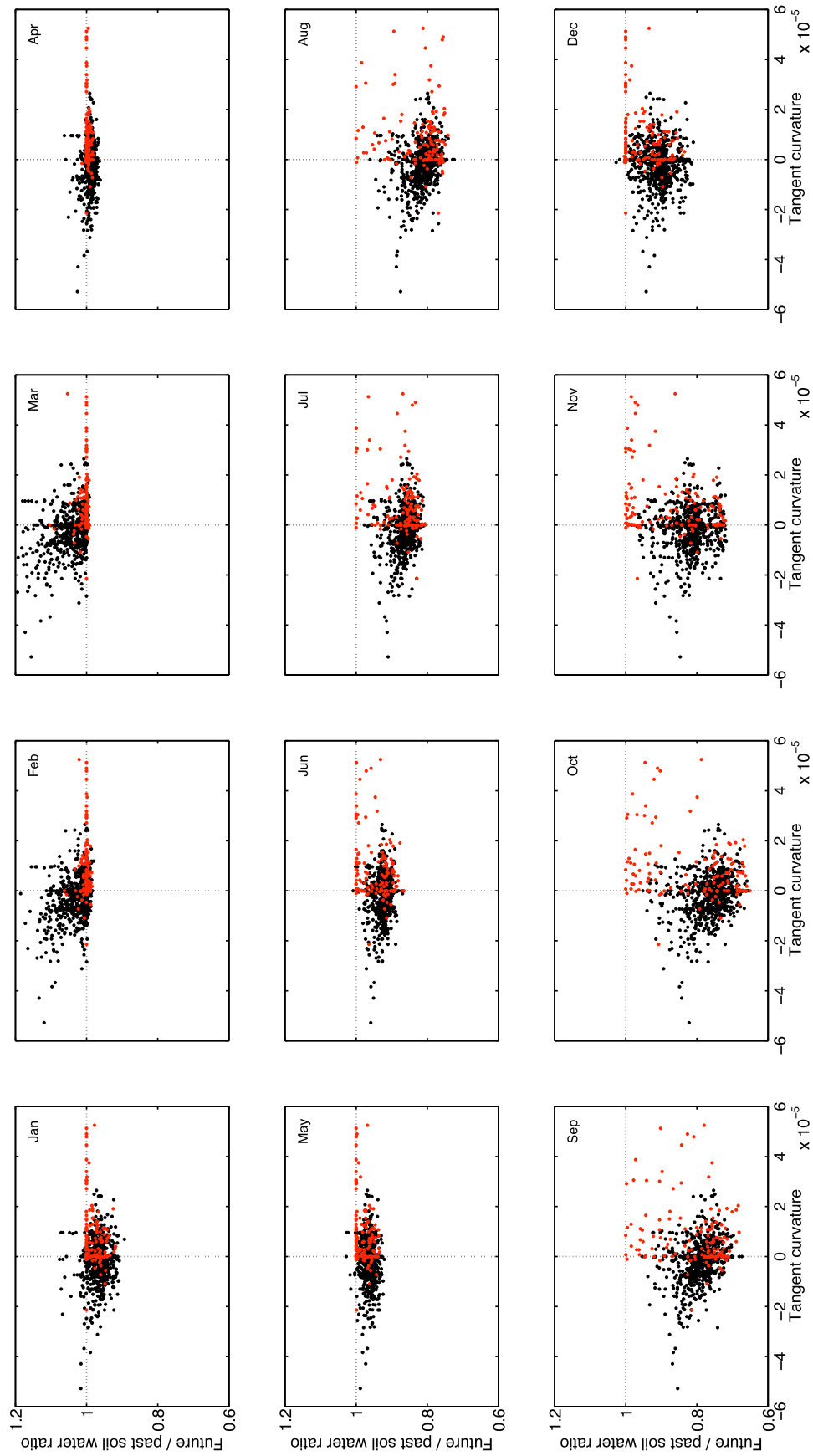


Figure 12. Scatterplot between the future/past surface soil water ratio and the tangent curvature for the channel (red points) and hillslope cells (black points). The analysis refers to the inset area of the catchment shown in Figure 11.

Table 5. Soil Parameters for the CLASS Model

	CRCM Grid Points			
	1	2	3	4
Layer 1 (0.00–0.10 m)				
K_z (m/s)	2.84×10^{-5}	2.84×10^{-5}	1.22×10^{-6}	1.46×10^{-6}
θ_s	0.37	0.37	0.48	0.47
Layer 2 (0.10–0.35 m)				
K_z (m/s)	3.05×10^{-5}	3.05×10^{-5}	1.10×10^{-6}	1.34×10^{-6}
θ_s	0.36	0.36	0.36	0.48
Layer 3 (0.35–4.10 m)				
K_z (m/s)	3.44×10^{-5}	3.44×10^{-5}	1.11×10^{-6}	1.30×10^{-6}
θ_s	0.36	0.36	0.48	0.48
Bedrock depth (m)	3.0	3.0	1.7	1.2

the two models is not the same. For CLASS, which was applied over the entire North American domain, some level of calibration was done for empirical relationships such as hydrological properties as a function of texture or snow thermal conductivity as a function of density, with field measurements from specific locations used to constrain and simplify complex physical relationships through linear or higher-order regressions, which are then assumed to apply in general.

[50] As can be seen in Figure 13, CLASS produces higher estimates than CATHY of surface and subsurface runoff throughout the annual cycle for both past and future simulations, with the greatest difference occurring at peak flow during snowmelt. The important factors contributing to these discrepancies in model prediction most likely include the degree of physical detail included in the surface and subsurface parameterizations and the differing spatial resolutions of the two models (affecting, for instance, the ability to capture important topographic features and subsurface heterogeneities that strongly influence the response of the catchment). In CLASS, surface runoff is described by a two-stage infiltration model where the first stage predicts the volume of infiltration until surface ponding begins and the second stage, which is a modified Green-Ampt model, describes the subsequent infiltration down to the root zone. Compared to a 1-D Richards equation, this simplified model can underestimate the infiltrated volume prior to runoff [Mein and Larson, 1973], and this underestimation is amplified for steeper slope angles if, as in CLASS, slopes are not accounted for [Chen and Young, 2006]. A 3-D Richards equation model such as CATHY provides additional byways for infiltration, through lateral subsurface moisture redistribution and, with surface coupling, through downslope re-infiltration.

[51] To further illustrate differences in response between the CLASS and CATHY models, Figure 14 shows the results on a daily time step for one year (1979) of the 30 year past climate simulation. It is evident, particularly during wet periods (February–March and late fall/early winter), that CLASS produces a more intense hydrograph response (higher peaks of shorter duration) and a lower recession component (normally associated with subsurface contributions to runoff). Subsurface runoff in CLASS is computed as the flow out of the third soil layer (from 0.35 to 4.10 m depth). The higher peak runoff in CLASS is also partly due to the lack of attenuating processes such as explicit river routing and lake storage. The two models are better matched during the drier summer period.

Table 6. Vegetation Parameters for the CLASS Model^a

	CRCM Grid Points			
	1	2	3	4
Needleleaf trees				
FCAN	0.41	0.03	0.09	0.14
ALVC	0.03	0.03	0.03	0.03
ALIC	0.23	0.23	0.23	0.23
LNZ0	0.68	0.66	0.66	0.67
LAMX	2.48	2.45	2.44	2.28
LAMN	1.01	1.05	1.06	0.95
CMAS (kg/m ²)	15.91	15.63	15.59	14.56
ROOT(m)	1.48	1.45	1.44	1.35
Broadleaf trees				
FCAN	0.42	0.96	0.82	0.26
ALVC	0.05	0.05	0.05	0.05
ALIC	0.29	0.29	0.29	0.29
LNZ0	0.68	0.69	0.68	0.35
LAMX	5.99	6.00	5.99	8.65
LAMN	0.50	0.50	0.50	0.72
CMAS (kg/m ²)	19.95	20.00	19.95	28.28
ROOT(m)	1.99	2.00	1.99	2.84
Crops				
FCAN	0.16	0.005	0.06	0.50
ALVC	0.06	0.06	0.06	0.06
ALIC	0.34	0.34	0.34	0.34
LNZ0	-2.52	-2.52	-2.52	-2.52
LAMX	4.00	4.00	4.00	3.22
LAMN	0.00	0.00	0.00	0.00
CMAS (kg/m ²)	2.00	2.00	2.00	1.61
ROOT(m)	1.20	1.20	1.20	0.96
Grass				
FCAN	0.004	0.005	0.02	0.05
ALVC	0.04	0.04	0.04	0.05
ALIC	0.29	0.28	0.29	0.31
LNZ0	-3.07	-3.27	-3.20	-3.36
LAMX	3.26	2.92	3.07	2.68
LAMN	3.26	2.92	3.07	2.68
CMAS (kg/m ²)	2.07	1.91	1.92	1.48
ROOT(m)	0.99	0.87	0.90	0.75
Urban				
FCAN	0.005	0.001	0.01	0.05
ALVC	0.09	0.09	0.09	0.09
ALIC	0.15	0.15	0.15	0.15
LNZ0	0.30	0.30	0.30	0.30
LAMX	na	na	na	na
LAMN	na	na	na	na
CMAS (kg/m ²)	na	na	na	na
ROOT(m)	na	na	na	na

^aHere na indicates not available.

5.2.2. Soil Water Storage

[52] Groundwater dynamics and storage influence near-surface soil moisture and surface runoff. Water table fluctuations interact with soil moisture in the root zone and can affect evapotranspiration. In land surface models, the parameterization of subsurface processes falls within three broad classes: multilayered and relatively shallow soil profile without an explicit representation of groundwater dynamics, multilayered and deep soil profile that accounts for groundwater fluctuations even without an explicit representation, and multilayered soil column coupled in some way to an aquifer model. The CLASS model, with its three-layer discretization of the soil profile and no consideration of the water table dynamics, falls into the first category. For the past and future climate scenario simulations described in section 5.2, the soil water storage computed by the CATHY and CLASS models within each of the three

Table 7. CLASS-Equivalent Parameterization of the CATHY Model for the Four CRCM Grid Points of the des Anglais Catchment

	Layer (Top to Bottom)						
	1–2	3–4	5	6	7	8	9–12
Layer thickness (m)	0.05–0.05	0.125–0.125	0.85	0.50	1.30	1.10	5.90–20–30–40
Grid point 1							
$K_h = K_z$ (m/s)	2.84×10^{-5}	3.05×10^{-5}	3.44×10^{-5}	3.44×10^{-5}	3.44×10^{-5}	5.0×10^{-8}	5.0×10^{-8}
$\theta_s >$	0.37	0.36	0.36	0.36	0.36	0.1	0.1
S_s (m^{-1})	1×10^{-5}	1×10^{-6}	1×10^{-6}				
Grid point 2							
$K_h = K_z$ (m/s)	2.84×10^{-5}	3.05×10^{-5}	3.44×10^{-5}	3.44×10^{-5}	3.44×10^{-5}	5.0×10^{-8}	5.0×10^{-8}
$\theta_s >$	0.37	0.36	0.36	0.36	0.36	0.1	0.1
S_s (m^{-1})	1×10^{-5}	1×10^{-6}	1×10^{-6}				
Grid point 3							
$K_h = K_z$ (m/s)	1.22×10^{-6}	1.10×10^{-6}	1.11×10^{-6}	1.11×10^{-6}	5.0×10^{-8}	5.0×10^{-8}	5.0×10^{-8}
$\theta_s >$	0.48	0.36	0.48	0.48	0.1	0.1	0.1
S_s (m^{-1})	1×10^{-5}	1×10^{-5}	1×10^{-5}	1×10^{-5}	1×10^{-6}	1×10^{-6}	1×10^{-6}
Grid point 4							
$K_h = K_z$ (m/s)	1.46×10^{-6}	1.34×10^{-6}	1.30×10^{-6}	5.0×10^{-8}	5.0×10^{-8}	5.0×10^{-8}	5.0×10^{-8}
$\theta_s >$	0.47	0.48	0.48	0.1	0.1	0.1	0.1
S_s (m^{-1})	1×10^{-5}	1×10^{-5}	1×10^{-5}	1×10^{-6}	1×10^{-6}	1×10^{-6}	1×10^{-6}

CLASS layers (0–0.10, 0.10–0.35, and 0.35–4.10 m) is plotted in Figure 15. CLASS and CATHY are in general agreement in terms of the intra-annual variability of moisture content in the first two soil layers, particularly for the top layer in which water variations are most directly affected by rainfall events and by diurnal temperature changes during interstorm periods. The largest differences between the two models occur in the third layer, with CATHY predicting wetter soil conditions over the entire simulation period and moisture fluctuations of much smaller amplitude. The causes of this behavior are underestimation of infiltration in CLASS (discussed in section 5.2.1), together with the absence of an underlying groundwater reservoir that results in faster depletion of the bottom layer (in CLASS the bedrock is assumed to be an impermeable stratum with no water storage capacity).

[53] CLASS and CATHY soil water storage, as well as runoff, are also analyzed in terms of mean monthly ratios (future climate over past climate), as plotted in Figure 16.

For the CLASS model, with a higher surface contribution to the hydrograph, the runoff ratio is more sensitive to the relative variation in total precipitation between the future and past simulations, with the highest ratios observed in February. In terms of soil water storage, the changes from past to future climate in CATHY are most strongly felt nearest to the surface (first and second soil layers) and are progressively dampened as soil depth increases (third layer). CLASS, on the other hand, shows a less systematic response from shallow to deep layers, reflecting in part this model's more compartmentalized treatment of the subsurface.

[54] Overall, the differences in response between CLASS and CATHY highlight the importance of resolving soil and water table dynamics as a continuum when aquifers are relatively shallow, as is the case, on average, for a significant portion of the des Anglais river basin. For instance, over a depth range between 1 and 5 m, *Kollet and Maxwell* [2008] found the land surface water and energy budgets to be very

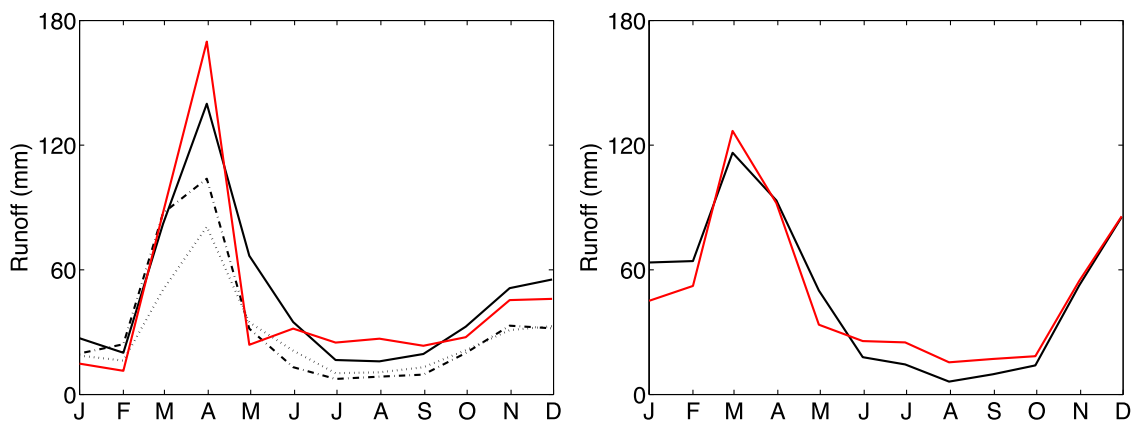


Figure 13. Mean monthly runoff for the (left) past and (right) future climate change projections: CLASS surface and subsurface runoff (red line) and CATHY catchment outlet discharge (black line). Figure 13 (left) also shows observed streamflow (dash-dotted line) and calibrated CATHY discharge (dotted line) for the period 1961–1990.

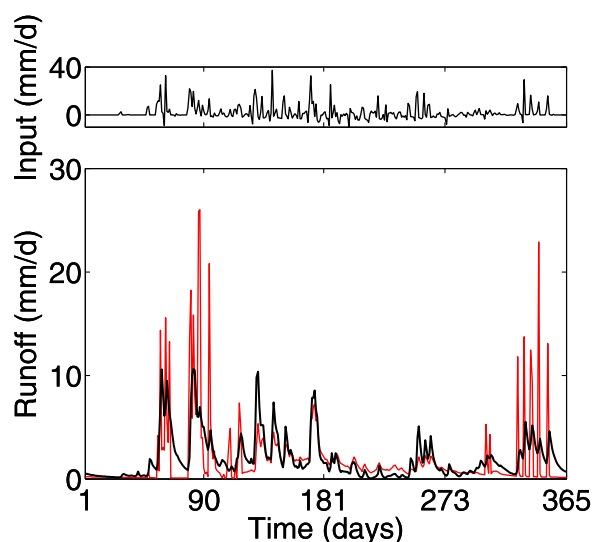


Figure 14. CLASS (red line) and CATHY (black line) daily runoff responses for year 1979 of the 30 year past climate simulation.

sensitive to groundwater storage for the Little Washita watershed in central Oklahoma. *York et al.* [2002] found that for the shallow aquifer (less than 2 m) of Mill Creek in northeastern Kansas the water table depth affected the process of evapotranspiration. And *Gutowski et al.* [2002] found that for the Konza Prairie watershed in Kansas, up to 33% of monthly evapotranspiration was derived from groundwater-supported exfiltration during dry periods. Further work is needed to assess the extent to which atmosphere and land surface processes are influenced by shallow and even deeper aquifers and to improve both the subsurface representations in models such as CLASS and the land surface-atmosphere dynamics (e.g., energy budget) in models such as CATHY.

[55] As a final remark, it is interesting to note that despite the caveats described earlier in comparing two models as different as CATHY and CLASS and despite significant differences in the detailed responses of the models, similarities in some other response characteristics, such as runoff timing and volume (Figures 13 and 14) and near-surface soil moisture fluctuations (Figure 15), suggest that the models have some elements of a common dynamic basis and that a river basin with the size of des Anglais (690 km²) is not a wholly inappropriate scale at which to intercompare and assess these two classes of model. Just as land surface models are evolving toward more sophisticated representations of subsurface flow processes, catchment and groundwater hydrological models are being extended to incorporate important exchange processes with the atmosphere, including energy and carbon fluxes. Both trends will enable simulation models to be more effectively used in assessing the impacts of climate change on freshwater resources.

6. Conclusions

[56] This paper has investigated the sensitivity of the hydrological response (river discharge, aquifer recharge, and soil water storage) of a small river basin to different

climate scenarios using a fully coupled numerical model of surface and subsurface flow. Climate variables (precipitation and minimum and maximum temperatures) were generated by the CRCM regional climate model for a past (1961–1990) and future (2041–2070) scenario. These data were further processed using the delta change transfer method and an observed data set to ensure representativeness of the synthetic data on a monthly basis. A statistical analysis using the Mann-Kendall test was performed for the past and future CRCM data sets. The results of this analysis revealed a significant positive trend in temperature (and hence in potential evapotranspiration) and no significant trend in precipitation. The positive trend in temperature was particularly strong for the winter and early summer months of the future scenario. The numerical model, calibrated first against integrated values of streamflow for one gauge of the catchment, was then verified against integrated values of streamflow at different points within the catchment and against distributed observations of water level depth located in parts of the catchment having different pedologic and geologic characteristics. For the single climate scenario used, this model setup enabled a preliminary investigation of the climate change impacts on different hydrologic response variables for the study basin.

[57] The results of the simulations for the des Anglais river basin show that at the main outlet the climate change impacts are most significant during the peak winter period because of the combination of more precipitation and higher temperature (and hence an increased rainfall to snowfall ratio) and during summer months because of a marked increase in temperature (and hence evaporation). The results also show significant spatiotemporal variations in the river discharge response to climate change owing to a different partitioning between the overland runoff and base flow components of the hydrograph, with the latter alleviating the marked decrease in discharge during the summer period. Recharge to the aquifer increases significantly during the winter season because of a higher rain/snow ratio caused by higher temperatures, whereas it decreases in the spring as a result of an earlier and less intense snowmelt and over the summer period because of increased evaporation. A spatial analysis of recharge patterns shows that the greatest variations are expected to occur, throughout the year, in the southern portion of the catchment, where the elevations are highest. This analysis also highlighted a possible reversal, during summer months, in groundwater-river interactions in response to groundwater storage deficits. Compared to river discharge and aquifer recharge, the water storage volumes are less sensitive to climate changes. Storage variations are most strongly felt nearest to the surface, which is directly exposed to fluctuations in precipitation and evapotranspiration, and are progressively dampened as soil depth increases. From a spatial analysis of soil moisture variations it was possible to observe organizational patterns that follow the topographic and pedologic characteristics of the catchment. Moreover, through an investigation of the relationship between the tangent curvature of the surface and the soil water variation, performed for a section of the catchment near the outlet, it was found that the hillslope cells located along convergent parts of the catchment tend to experience an increase in soil moisture content in February and March in response to

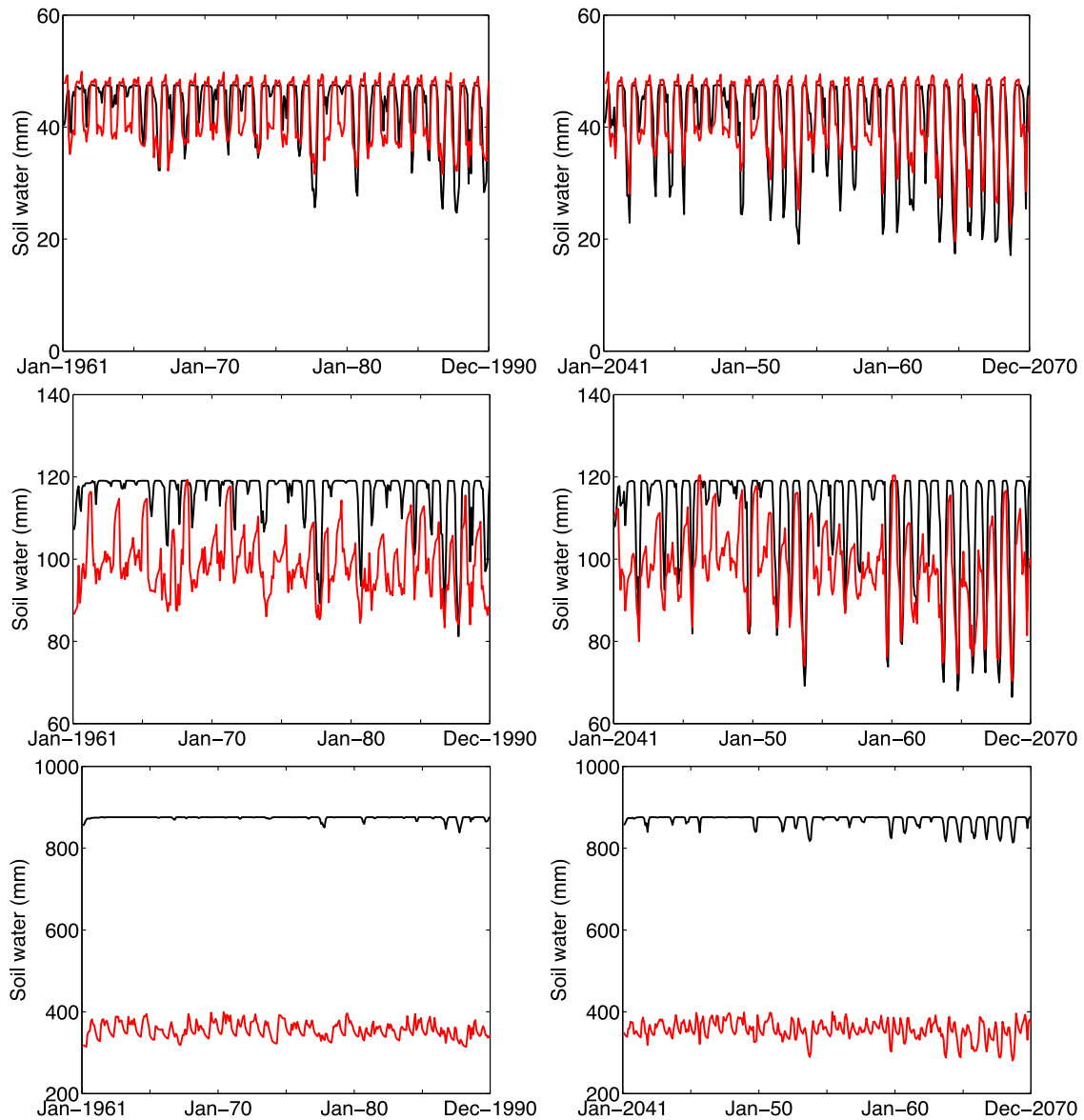


Figure 15. Monthly soil water content in the (top) 0–0.10 m, (middle) 0.10–0.35 m, and (bottom) 0.35–4.10 m CLASS layers for the (left) past and (right) future climate change projections: CLASS (red line) and CATHY (black line).

climate change and less variation in the late summer and early fall (August to October).

[58] An additional objective of the study was to compare the predictions obtained with CLASS, the land surface scheme that is coupled to the CRCM model, to those from the CATHY hydrological model for past and future climate change projections. Differences in runoff and soil water storage response were used to highlight some of the key differences in the models. For instance, we found that CLASS produces higher estimates than CATHY of surface and subsurface runoff throughout the annual cycle for both past and future scenarios, with the greatest difference occurring at the peak flow during snowmelt. The key factors contributing to these discrepancies were the different degrees of physical detail included in the surface and subsurface parameterizations (1-D Green-Ampt model versus

3-D Richards equation) and the different spatial resolutions of the two models, which affect the ability to capture important topographic features and subsurface heterogeneities that strongly influence the response of the catchment (e.g., lateral subsurface moisture redistribution). For soil water storage, CLASS and CATHY were found to be in general agreement in terms of the intra-annual variability of moisture content in the first two soil layers (0–0.10 and 0.10–0.35 m), particularly for the top layer, in which water variations are most directly affected by rainfall events and by diurnal temperature changes during interstorm periods. The largest differences between the two models occur in the third layer (0.35–4.10 m), with CATHY predicting wetter soil conditions over the entire simulation period and moisture fluctuations of much smaller amplitude. The probable causes of this behavior are the underestimation of

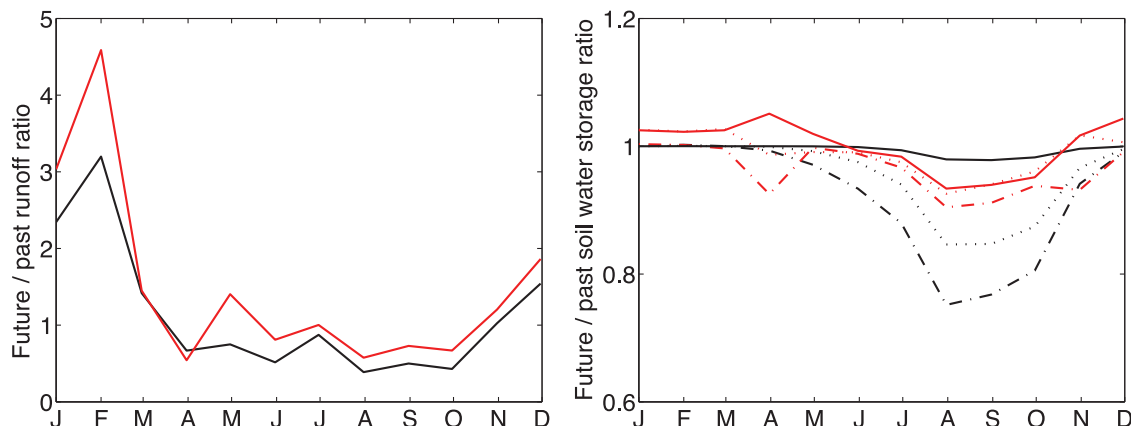


Figure 16. Ratios of (left) mean monthly discharge and (right) soil water content between future and past climates: CLASS (red lines) and CATHY (black lines). Soil storage results are shown for the 0–0.10 m (dash-dotted lines), 0.10–0.35 m (dotted lines), and 0.35–4.10 m (solid lines) CLASS layers.

infiltration in CLASS and the absence of an underlying groundwater reservoir, which results in faster depletion of the bottom layer.

[59] **Acknowledgments.** We acknowledge the financial support of the Ouranos Consortium and the Natural Sciences and Engineering Research Council of Canada (grant CRDPJ-319,968-04). The CRCM data has been generated and supplied by Ouranos, with CGCM driving data made available by the Canadian Center for Climate Modeling and Analysis (CCCma). We thank the reviewers for their detailed and very helpful comments.

References

- Abrahams, A. D., G. Li, and A. J. Parsons (1994), Rill hydraulics on a semi-arid hillslope, southern Arizona, *Earth Surf. Processes Landforms*, *21*(1), 35–47, doi:10.1002/(SICI)1096-9837(199601).
- Anderson, M. P., and W. W. Woessner (1992), *Applied Groundwater Modeling: Simulation of Flow and Advective Transport*, 381 pp., Academic, New York.
- Arnell, N. W., D. A. Hudson, and R. G. Jones (2003), Climate change scenarios for a regional climate model: Estimating change in runoff in southern Africa, *J. Geophys. Res.*, *108*(D16), 4519, doi:10.1029/2002JD002782.
- Arora, V. K., and G. J. Boer (2001), Effects of simulated climate change on the hydrology of major river basins, *J. Geophys. Res.*, *106*(D4), 3335–3348, doi:10.1029/2000JD900620.
- Bathurst, J. C. (1986), Physically-based distributed modelling of an upland catchment using the Système Hydrologique Européen, *J. Hydrol.*, *87*(1-2), 79–102, doi:10.1016/0022-1694(86)90116-2.
- Bathurst, J. C. (1993), Flow resistance through the channel network, in *Channel Network Hydrology*, edited by K. Beven and M. J. Kirkby, pp. 69–98, John Wiley, New York.
- Boone, A., et al. (2004), The Rhone-aggregation land surface scheme intercomparison project: An overview, *J. Clim.*, *17*(1), 187–208, doi:10.1175/1520-0442(2004)017.
- Bowling, L. C., et al. (2003), Simulation of high latitude hydrological processes in the Torne–Kalix basin: PILPS Phase 2(e): 1: Experimental description and summary intercomparisons, *Global Planet. Change*, *38*(1-2), 1–30, doi:10.1016/S0921-8181(03)00003-1.
- Brubaker, K. L., and D. Entekhabi (1996), Analysis of feedback mechanisms in land-atmosphere interaction, *Water Resour. Res.*, *32*(5), 1343–1357.
- Caballero, Y., S. Voirin-Morel, F. Habets, J. Noilhan, P. LeMoigne, A. Lehenaff, and A. Boone (2007), Hydrological sensitivity of the Adour-Garonne river basin to climate change, *Water Resour. Res.*, *43*, W07448, doi:10.1029/2005WR004192.
- Camporese, M., C. Paniconi, M. Putti, and S. Orlandini (2010), Surface-subsurface flow modeling with path-based runoff routing, boundary condition-based coupling, and assimilation of multisource observation data, *Water Resour. Res.*, *46*, W02512, doi:10.1029/2008WR007536.
- Caya, D., and R. Laprise (1999), A semi-implicit semi-Lagrangian regional climate model: The Canadian RCM, *Mon. Weather Rev.*, *127*(3), 341–362.
- Chen, L., and M. H. Young (2006), Green-Ampt infiltration model for sloping surfaces, *Water Resour. Res.*, *42*, W07420, doi:10.1029/2005WR004468.
- Chiew, F. H., J. Teng, J. Vaze, D. A. Post, J. M. Perraud, D. G. C. Kirono, and N. R. Viney (2009), Estimating climate change impact on runoff across southeast Australia: Method, results, and implications of modeling method, *Water Resour. Res.*, *45*, W10414, doi:10.1029/2008WR007338.
- Christensen, J. H., and O. B. Christensen (2007), A summary of the PRUDENCE model projections of changes in European climate by the end of this century, *Clim. Change*, *81*, suppl. 1, 7–30, doi:10.1007/s10584-006-9210-7.
- Clapp, R. B., and G. M. Hornberger (1978), Empirical equations for some soil hydraulic properties, *Water Resour. Res.*, *14*(4), 601–604, doi:10.1029/WR014i004p00601.
- Cosby, B. J., G. M. Hornberger, R. B. Clapp, and R. Ginn (1984), A statistical exploration of the relationships of soil moisture characteristics to the physical properties of soils, *Water Resour. Res.*, *20*(6), 682–690, doi:10.1029/WR020i006p00682.
- Côté, M.-J., Y. Lachance, C. Lamontagne, M. Nasteve, R. Plamondon, and N. Roy (2006), Atlas du bassin versant de la rivière Chateauguay, technical report, Minist. du Dev. durable, de l'Environ. et des Parcs, Quebec, Que., Canada.
- Dooge, J. C. I., M. Bruen, and B. Parmentier (1999), A simple model for estimating the sensitivity of runoff to long-term changes in precipitation without change in vegetation, *Adv. Water Resour.*, *23*(2), 153–163, doi:10.1016/S0309-1708(99)00019-6.
- Eckhardt, K., and U. Ulbrich (2003), Potential impacts of climate change on groundwater recharge and streamflow in a central European low mountain range, *J. Hydrol.*, *284*(1-4), 244–252.
- Eltahir, E. A. B. (1998), A soil moisture–rainfall feedback mechanism: 1. Theory and observations, *Water Resour. Res.*, *34*(4), 765–776, doi:10.1029/97WR03499.
- Emmett, W. W. (1978), Overland flow, in *Hillslope Hydrology*, edited by M. J. Kirkby, p. 145–176, John Wiley, New York.
- Fan, Y., G. Miguez-Macho, C. P. Weaver, R. Walko, and A. Robock (2007), Incorporating water table dynamics in climate modeling: 1. Water table observations and equilibrium water table simulations, *J. Geophys. Res.*, *112*, D10125, doi:10.1029/2006JD008111.
- Flato, G. M., and G. J. Boer (2001), Warming asymmetry in climate change simulations, *Geophys. Res. Lett.*, *28*(1), 195–198, doi:10.1029/2000GL012121.
- Furman, A. (2008), Modeling coupled surface-subsurface flow processes: A review, *Vadose Zone J.*, *7*(2), 741–756, doi:10.2136/vzj2007.0065.
- Gleick, P. H. (1989), Climate change, hydrology, and water resources, *Rev. Geophys.*, *27*(3), 329–344, doi:10.1029/RG027i003p00329.

- Green, W. H., and G. A. Ampt (1911), Studies on soil physics: I. Flow of air and water through soils, *J. Agric. Sci.*, 4(1), 1–24.
- Gulden, L. E., E. Rosero, Z.-L. Yang, M. Rodell, C. S. Jackson, G.-Y. Niu, P. J.-F. Yeh, and J. Famiglietti (2007), Improving land-surface model hydrology: Is an explicit aquifer model better than a deeper soil profile?, *Geophys. Res. Lett.*, 34, L09402, doi:10.1029/2007GL029804.
- Gutowski, W. J., C. J. Vörösmarty, M. Person, Z. Ötles, B. Fekete, and J. York (2002), A Coupled Land-Atmosphere Simulation Program (CLASP): Calibration and validation, *J. Geophys. Res.*, 107(D16), 4283, doi:10.1029/2001JD000392.
- Hay, L. E., R. L. Wilby, and G. H. Leavesley (2000), A comparison of delta change and downscaled GCM scenarios for three mountainous basins in the United States, *J. Am. Water Resour. Assoc.*, 36(2), 387–398, doi:10.1111/j.1752-1688.2000.tb04276.x.
- Hirsh, R. M., J. R. Slack, and R. A. Smith (1982), Techniques of trend analysis for monthly water quality data, *Water Resour. Res.*, 18(1), 107–121.
- Intergovernmental Panel on Climate Change (IPCC) (2000), *Emissions Scenarios: A Special Report of Working Group III of the Intergovernmental Panel on Climate Change*, edited by N. Nakicenovic and S. Swart, 612 pp., Cambridge Univ. Press, Cambridge, U. K.
- Intergovernmental Panel on Climate Change (IPCC) (2007), *Climate Change 2007: Impacts, Adaptation and Vulnerability. Contributions of Working Group II to the Fourth Assessment Report of the Intergovernmental Panel on Climate Change*, edited by M. L. Parry et al., Cambridge Univ. Press, Cambridge, U. K.
- Jones, J. P., E. A. Sudicky, and R. G. McLaren (2008), Application of a fully-integrated surface-subsurface flow model at the watershed-scale: A case study, *Water Resour. Res.*, 44, W03407, doi:10.1029/2006WR005603.
- Jyrkama, M. I., and J. F. Sykes (2007), The impact of climate change on spatially varying groundwater recharge in the Grand River watershed (Ontario), *J. Hydrol.*, 338(3–4), 237–250, doi:10.1016/j.jhydrol.2007.02.036.
- Kendall, M. G. (1975), *Rank Correlation Measures*, Charles Griffin, London.
- Kollet, S. J., and R. M. Maxwell (2008), Capturing the influence of groundwater dynamics on land surface processes using an integrated, distributed watershed model, *Water Resour. Res.*, 44, W02402, doi:10.1029/2007WR006004.
- Lamontagne, L. (2005), Base de données sur les propriétés physiques des sols du bassin versant de la rivière Chateauguay, report, Pedol. and Precis. Agric. Lab., *Agric. and Agri-Food Can.*, Quebec, Que., Canada.
- Lee, D. H., and L. M. Abriola (1999), Use of the Richards equation in land surface parameterizations, *J. Geophys. Res.*, 104(D22), 27,519–27,526.
- Liang, X., Z. Xie, and M. Huang (2003), A new parameterization for surface and groundwater interactions and its impact on water budgets with the variable infiltration capacity (VIC) land surface model, *J. Geophys. Res.*, 108(D16), 8613, doi:10.1029/2002JD003090.
- Manabe, S., J. Smagorinsky, and R. Strickler (1965), Simulated climatology of a general circulation model with a hydrologic cycle, *Mon. Weather Rev.*, 93(12), 769–798.
- Mann, H. B. (1945), Non-parametric tests against trend, *Econometrica*, 13(3), 245–259, doi:10.2307/1907187.
- Maxwell, R. M., F. K. Chow, and S. J. Kollet (2007), The groundwater–land-surface–atmosphere connection: Soil moisture effects on the atmospheric boundary layer in fully-coupled simulations, *Adv. Water Resour.*, 30(12), 2447–2466, doi:10.1016/j.advwatres.2007.05.018.
- Mein, R. G., and C. L. Larson (1973), Modeling infiltration during a steady rain, *Water Resour. Res.*, 9(2), 384–394.
- Mitasova, H., and J. Hofierka (1993), Interpolation by regularized spline with tension, II, Application to terrain modeling and surface geometry analysis, *Math. Geol.*, 25(6), 657–669, doi:10.1007/BF00893172.
- Music, B., and D. Caya (2007), Evaluation of the hydrological cycle over the Mississippi river basin as simulated by the Canadian Regional Climate Model (CRCM), *J. Hydrometeorol.*, 8(5), 969–988, doi:10.1175/JHM627.1.
- Nash, J. E., and J. V. Sutcliffe (1970), River flow forecasting through conceptual models. Part 1: A discussion of principles, *J. Hydrol.*, 10(3), 282–290, doi:10.1016/0022-1694(70)90255-6.
- Oudin, L., F. Hervieu, C. Michel, C. Perrin, V. Andréassian, F. Anctil, and C. Loumagne (2005), Which potential evapotranspiration input for a lumped rainfall-runoff model? Part 2—Towards a simple and efficient potential evapotranspiration model for rainfall-runoff modelling, *J. Hydrol.*, 303(1–4), 290–306, doi:10.1016/j.jhydrol.2004.08.026.
- Pitman, A. J. (2003), The evolution of, and revolution in, land surface schemes designed for climate models, *Int. J. Climatol.*, 23(5), 479–510, doi:10.1002/joc.893.
- Prudhomme, C., D. Jakob, and C. Svensson (2003), Uncertainty and climate change impact on the flood regime of small UK catchments, *J. Hydrol.*, 277(1–2), 1–23, doi:10.1016/S0022-1694(03)00065-9.
- Quilbé, R., A. N. Rousseau, J.-S. Moquet, S. Savary, S. Ricard, and M. S. Garbouj (2008), Hydrological responses of a watershed to historical land use evolution and future land use scenarios under climate change conditions, *Hydrol. Earth Syst. Sci.*, 12(1), 101–110, doi:10.5194/hess-12-101-2008.
- Riette, S., and D. Caya (2002), Sensitivity of short simulations to the various parameters in the new CRCM spectral nudging, in *Research Activities in Atmospheric and Oceanic Modelling*, edited by H. Ritchie, Rep. 32, pp. 7.39–7.40, World Meteorol. Organ., Geneva, Switzerland.
- Rivington, M., D. Miller, K. B. Matthews, G. Russell, G. Bellocchi, and K. Buchan (2008), Evaluating regional climate model estimates against site-specific observed data in the UK, *Clim. Change*, 88(2), 157–185, doi:10.1007/s10584-007-9382-9.
- Salvucci, G. (1997), Soil and moisture independent estimation of stage-two evaporation from potential evaporation and albedo or surface temperature, *Water Resour. Res.*, 33(1), 111–122.
- Scibek, J., and D. M. Allen (2006), Modeled impacts of predicted climate change on recharge and groundwater levels, *Water Resour. Res.*, 42, W11405, doi:10.1029/2005WR004742.
- Scinocca, J. F., N. A. McFarlane, M. Lazare, J. Li, and D. Plummer (2008), The CCCma third generation AGCM and its extension into the middle atmosphere, *Atmos. Chem. Phys.*, 8(23), 7055–7074, doi:10.5194/acp-8-7055-2008.
- Sen, P. K. (1968), Estimates of the regression coefficient based on Kendall's tau, *J. Am. Stat. Assoc.*, 63(324), 1379–1389, doi:10.2307/2285891.
- Singh, V. P., and D. A. Woolhiser (2002), Mathematical modeling of watershed hydrology, *J. Hydrol. Eng.*, 7(4), 270–292, doi:10.1061/(ASCE)1084-0699(2002)7:4(270).
- Sulis, M., C. Paniconi, and M. Camporese (2010), Impact of grid resolution on the integrated and distributed response of a coupled surface-subsurface hydrological model for the des Anglais catchment, Quebec, *Hydrol. Processes*, in press, doi:10.1002/hyp.7941.
- Tague, C., G. Grant, M. Farrell, J. Choate, and A. Jefferson (2008), Deep groundwater mediates streamflow response to climate warming in the Oregon Cascades, *Clim. Change*, 86(1–2), 189–210, doi:10.1007/s10584-007-9294-8.
- Toews, M. W., and D. M. Allen (2009), Evaluating different GCMs for predicting spatial recharge in an irrigated arid region, *J. Hydrol.*, 374(3–4), 265–281, doi:10.1016/j.jhydrol.2009.06.022.
- Tremblay, T. (2006), Hydrostratigraphie et géologie du Quatremaire dans le bassin-versant de la rivière Chateauguay, Québec, M.S. thesis, 224 pp., Univ. Que. à Montréal, Montreal, Que., Canada.
- Turcotte, R., L.-G. Fortin, V. Fortin, J.-P. Fortin, and J.-P. Villeneuve (2004), Operational analysis of the spatial distribution and the temporal evolution of the snowpack water equivalent in southern Quebec, Canada, *Nord. Hydrol.*, 38(3), 211–234, doi:10.2166/nh.2007.009.
- van Genuchten, M. T., and D. R. Nielsen (1985), On describing and predicting the hydraulic properties of unsaturated soils, *Ann. Geophys.*, 3(5), 615–628.
- van Roosmalen, L., T. O. Sonnenborg, and K. H. Jensen (2009), The impact of climate and land use change on the hydrology of a large-scale agricultural catchment, *Water Resour. Res.*, 45, W00A15, doi:10.1029/2007WR006760.
- Verseghy, D. L. (1991), CLASS—A Canadian land surface scheme for GCMs: I. Soil model, *Int. J. Climatol.*, 11(4), 111–133, doi:10.1002/joc.3370110202.
- Verseghy, D. L., N. A. McFarlane, and M. Lazare (1993), CLASS—A Canadian land surface scheme for GCMs: II. Vegetation model and coupled runs, *Int. J. Climatol.*, 13(4), 347–370, doi:10.1002/joc.3370130402.
- von Storch, H., and A. Navarra (Eds.) (1995), *Analysis of Climate Variability: Applications of Statistical Techniques*, Springer-Verlag, New York.
- Wang, S., R. F. Grant, D. L. Verseghy, and T. A. Black (2002), Modelling carbon-coupled energy and water dynamics of a boreal aspen forest in a general circulation model land surface scheme, *Int. J. Climatol.*, 22(10), 1249–1265, doi:10.1002/joc.776.
- Western, A. W., R. B. Grayson, G. Blöschl, G. R. Willgoose, and T. A. McMahon (1999), Observed spatial organization of soil moisture and its

- relation to terrain indices, *Water Resour. Res.*, 35(3), 797–810, doi:10.1029/1998WR900065.
- Wilby, R. L., and I. Harris (2006), A framework for assessing uncertainties in climate change impacts: Low-flow scenarios for the River Thames, UK, *Water Resour. Res.*, 42, W02419, doi:10.1029/2005WR004065.
- Wilby, R. L., and T. M. L. Wigley (1997), Downscaling general circulation model output: A review of methods and limitations, *Prog. Phys. Geogr.*, 21(4), 530–548, doi:10.1177/030913339702100403.
- Wilson, M. F., and A. Henderson-Sellers (1985), A global archive of land cover and soils data for use in general circulation climate models, *J. Climatol.*, 5(2), 119–143.
- Yeh, P. J.-F., and E. A. B. Eltahir (2005), Representation of water table dynamics in a land surface scheme. Part I: Model development, *J. Clim.*, 18(12), 1861–1880.
- York, J. P., M. Person, W. J. Gutowski, and T. C. Winter (2002), Putting aquifers into atmospheric simulation models: An example from the Mill Creek Watershed, northeastern Kansas, *Adv. Water Resour.*, 25(2), 221–238, doi:10.1016/S0309-1708(01)00021-5.
- Yue, S., P. Pilon, B. Phinney, and G. Cavadias (2002), The influence of autocorrelation on the ability to detect trend in hydrological series, *Hydrol. Processes*, 16(9), 1807–1829, doi:10.1002/hyp.1095.
- Zhang, X., W. D. Hogg, and E. Mekis (2000), Temperature and precipitation trends in Canada during the 20th century, *Atmos. Ocean*, 38(3), 395–429.
- Zhang, X., K. D. Harvey, W. D. Hogg, and T. R. Yuzyk (2001), Trends in Canadian streamflow, *Water Resour. Res.*, 37(4), 987–998.
-
- D. Chaumont and R. Harvey, Ouranos Consortium on Regional Climatology and Adaptation to Climate Change, 550 Sherbrooke West, West Tower, 19th floor, Montreal, QC H3A 1B9, Canada. (chaumont.diane@ouranos.ca; harvey.richard@ouranos.ca)
- C. Paniconi and M. Sulis, Centre Eau, Terre et Environnement, Institut National de la Recherche Scientifique, 490 rue de la Couronne, Quebec, QC G1K 9A9, Canada. (claudio.paniconi@ete.inrs.ca; mauro.sulis@ete.inrs.ca)
- C. Rivard, Geological Survey of Canada, 490 rue de la Couronne, Quebec, QC G1K 9A9, Canada. (crivard@NRCan.gc.ca)